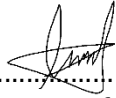# S U

Universitetet i Stavanger

Faculty of Science and Technology

MASTER'S THESIS

Study program/specialization: MSc in Marine and Offshore Technology	Spring semester, 2021 Open / ~~Restricted~~ access
Author: Mert Kaptan	.... (signature of author)

Supervisor:
      Dr. Bjørn Skaare
Co-Supervisors:
      Dr. Zhiyu Jiang, Prof. Muk Chen Ong	

Title: Comparison of spar and semi-submersible floating wind turbine concepts with respect to seasickness of the maintenance personnel	
Credits: 30 ECTS	
Keywords: Floating offshore wind; rigid body motions; response amplitude operator; seasickness; workability	Number of pages: 86 Stavanger, June 07, 2021

Abstract

Floating offshore wind turbines (FOWTs) are remotely located structures that are operating without humans on board. The technicians are expected to be on board from time to time throughout the life cycle of FOWTs for maintenance activities such as regular inspections, fault-findings, component changing etc. Due to their remote location, FOWTs are usually subjected to harsh environmental conditions that may cause large motions on the platform. Such motions may obstruct access to the platform and the maintenance work that is going to be conducted on the platform by the technicians. To address the problem and define the objectives, a literature study is conducted on the maintenance process of the FOWTs, the effects of platform motions on the humans located on the structure. The standards and regulations regarding the seakeeping performance of the vessels for human effectiveness and health are demonstrated. Then the motions of the floaters, modelling of the offshore sea conditions and the working principle of the software used are covered with a compact theory. A methodology is developed for the frequency domain to simulate the motions of the floaters in offshore conditions and model the motion exposure of the personnel on the structure. The developed methodology is utilised for three chosen study case floaters. OC3-Hywind, CSC-Semisubmersible and WindFloat are selected for comparative simulation studies where the workability of the technicians on each floater is investigated under different loading conditions. The load cases are modelled with both the JONSWAP and the Torsethaugen wave spectra based on hindcast data from two locations that are relevant for FOWT deployment. The conducted research is presented as a journal paper within this thesis. Additional results which were not included in the paper such as the investigation of the developed methodology and the expected extreme accelerations on the floaters are presented within the thesis. Instantaneous accelerations expected on each floater are graded regarding criteria for the human comfort reactions to vibration environments. Conclusions are made based on the findings from the comparative studies. The thesis is finalised with recommendations for further work.

ii

Acknowledgements

I would like to thank Dr Bjørn Skaare for the opportunity to work on such an interesting topic and for his effort to provide access to such data which made this work even more interesting. I would also like to thank him for guiding me throughout the challenges of this work while teaching me how to fish rather than giving me a fish in other words. Publishing a journal paper within this thesis, undeniably wouldn't be possible without his contribution.

I would like to extend my deep gratitude to Dr. Zhiyu Jiang whose valuable advice on the motion analysis of FOWTs and patient guidance to the simulation tools are the keys to the completion of this whole project. Additionally, I would like to express my appreciations to him once again, especially for his efforts to help and guide me out of office hours.

I would like to thank Prof. Dr. Muk Chen Ong for providing me with such a topic under the supervision of great researchers and his motivational contribution that helped me to do my best throughout this work. I am also appreciated for his organizational arrangements such as a laboratory that we were provided to work with well-equipped hardware.

Lastly, I would like to express my deepest appreciations to my family and my friends for their endless aid and support, and Jennie for her love and encouragement. Without her company and support, this work would have never been accomplished.

M. Kaptan

Stavanger, Norway
June, 2021

Table of Contents

List of Figures

List of Tables

Chapter 1

1. Introduction

The annual energy consumption of the world is increasing every year in correlation with the growth of the population. For a long time, traditional power sources such as coal, oil and gas have been playing an important role to meet the gradually increasing energy demand. For instance, a total of 26700 TWh energy has been generated in 2018 and carbon-based sources; coal, oil and gas made up approximately 64% of it while nuclear energy and renewables (hydro, solar, wind, etc.) remained at 10% and 26% respectively [1]. However, with the increase of awareness towards the environmental problems and the sustainability related to the usage of traditional energy sources, the source of attention in terms of energy supply is shifting to renewable energy sources.

One of the most promising renewable energy sources; the wind was started to be used as a storable source of energy in the late 19th century with the invention of wind turbines which is a complex system that transforms wind's kinetic energy into electricity. A wind turbine consists of a set of blades that are forced to rotate around a rotor which is connected to a shaft of a generator within the nacelle. The nacelle is located on a certain height level of a tower that allows blades to reach desired wind properties. Conventionally, wind turbines are installed on the land, hence towers are usually fixed directly to the ground or mounted on a relatively simple foundation such as wide concrete platforms, monopiles, etc. However, the area required to build enough wind farms on the land to replace the traditional energy sources with wind energy does not seem sustainable either considering the regulations related to noise and visual pollution. Therefore, oceans and seas were started to be considered as a possible site for wind turbines and the first wind farm consitsing of 11 wind turbines with a total capacity of 4.95 MW was built in 1991 in shallow waters at the coast of Vindeby/Denmark. The chosen site in Denmark had a maximum water depth of 4 meters, hence a gravity-based simple concrete platform was used as the foundation for each tower. The development of offshore wind technology speeded up in the following years and naturally cost-efficient solutions were explored for deeper waters as well. Some of the foundation types developed for offshore wind turbines are displayed in **Figure 1.1**.
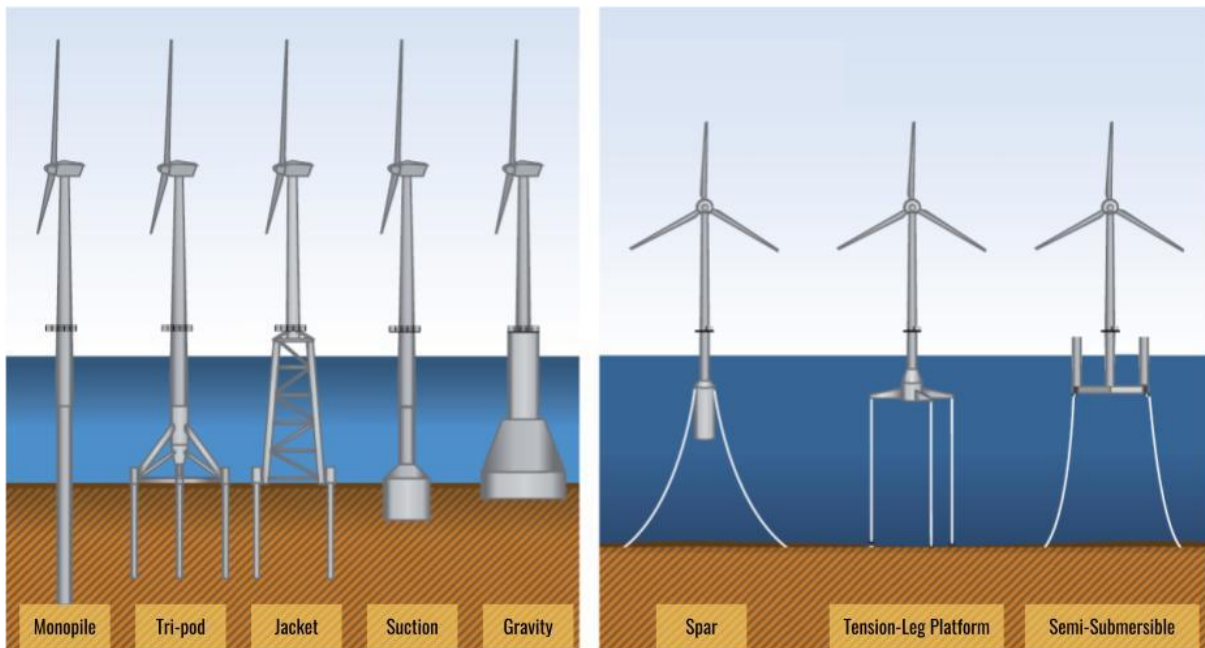
Figure 1.1: Conventional offshore wind turbine foundations and floating concepts (Edenhofer et al., 2012)**.**

Until today, bottom-fixed turbines have been installed up to 60 meters of water depth. The deepest installation is The Beatrice offshore wind farm with a total capacity of 588 MW which consists of 84 wind turbines each mounted on a jacket foundation, located off the coast of Scotland, as per the author's knowledge. However, years of technological advancements and experience have shown that 60 meters of sea depth may be regarded as a cut-off level for bottom-fixed offshore wind turbines [2]. Considering that almost 80% of the world's offshore wind potential resources are in waters deeper than 60 meters [3], the development of a floating offshore wind turbine concept was inevitable. Accordingly, profitable solutions have been developed for floating offshore wind in the early 2000s. The feasibility of the first preliminary floating offshore wind design (spar-type) has been tested with the deployment of a 2.3 MW demonstration unit (Hywind Demo) in 2009. Following 8 years of successful operation of the prototype validated the concept and led to the first wind farm project, Hywind Scotland. Until now, Hywind Scotland stands as the only operational floating offshore wind farm in the world which indicates that floating offshore wind as a technology is still immature with a lot of room to progress.

Floaters such as spar, semi-submersible and tension-leg platform (TLP) were already well-known concepts from the oil&gas industry after years of successful operations [4]. Creating a robust and stable structure to operate in harsh environmental conditions was already a solved engineering problem while keeping the project economically feasible is still the biggest

challenge. Besides, offshore wind turbines are designed to be operated without humans on board, unlike oil&gas platforms. So, a crew of maintenance personnel are transferred to the asset when in need, usually with a daily charted vessel. In order to achieve the lowest downtime possible and reduce additional costs due to rescheduling of the operations on floating offshore wind turbines (FOWTs), it is important to make sure that maintenance personnel can safely travel to the platform and conduct their work onboard in the pre-determined period. The comfort and well-being of the humans during their stay on the floater are as important as the safety of the operation. Therefore, a methodological study is conducted to investigate the comfort of maintenance personnel on different floater designs based on the selected motion criteria in this thesis. Further in this chapter, the background and motivation, problem definition and objectives will be explained. The structure of the thesis is presented and an overview of previous work on the topic is given.

1.1. Background and Motivation

Floating offshore wind turbines (FOWTs) are less dependent on water depth in terms of the costs and the design of the foundation compared to bottom-fixed structures and they are usually designed to be located further offshore to reach higher wind speed with less turbulence. Naturally, FOWTs are subjected to larger loads in general due to harsher environmental conditions which may lead to many additional challenges in the operation and maintenance (O&M) context. For instance, transport time to the asset may remarkably be higher compared to bottom-fixed structures because of the remote location of the floaters. Besides, higher wind speed and larger waves may exceed the operational limits of the transfer vessels which can cause longer downtimes on the asset due to waiting for a weather window. In addition to that, since floaters are not fixed structures, they are expected to experience a larger amplitude of motions which may also jeopardise the work of the maintenance personnel.

Currently, a conventionalized FOWT design has not been reached. Even though spar and semi-submersible are well-studied concepts and they are technologically developed; the connection between the acceleration level and human discomfort is not clear yet. Current researches in the field are putting a heavy emphasis on further understanding of the structural behaviour and responses of FOWTs in different operating conditions [5]. Wind turbines are set to the parked position during the maintenance of the FOWTs to reduce the wind loads. In that condition, the

dynamic response of the FOWT is dominated by wave and current loads and the wind's drag force on the tower and blades is negligible.

It is crucial to have a good understanding of the floater's motions to evaluate the possible effects of these motions on the safety, comfort and effectiveness of the personnel on the platform. Sustaining the comfort and effectiveness of the maintenance personnel would allow them to finish the maintenance in the desired time. This would reduce the downtime of the asset and prevent the longer loss of production and the additional costs due to re-scheduling of the whole operation. Considering, such transfer vessels are usually not owned by the operator companies, it would save the budget from a potential additional renting cost.

1.2. Problem and Objective Definitions

The problem of the motion exposure of the humans located on a FOWT can be considered as a vibration signal which is the rigid body motion of the floater in this case. Since the rotor is parked (no thrust) during the maintenance activity, wind loads on the blades and the tower are assumed negligible. Therefore, the tower flexibility is ignored. The research methodology is based on the numerical study conducted in the frequency domain to determine the FOWT's response in irregular sea states and to assess the response according to the selected limiting motion criteria. Statistical responses of the floaters are derived from the response amplitude operators (RAOs) with the assumption that sea states are stationary in the determined reference period. RAOs of the floaters are calculated in the frequency domain by using a potential theory code called Wadam and the calculated RAOs of the selected FOWT concepts are validated against published numerical and experimental studies. Wadam is a commercial hydrodynamic analysis tool that provides solutions to the radiation-diffraction problem and linearized Morison's equation for a 3-D panel model or a beam model [6].

The scope of the thesis is focused on two major studies. In the first part, which is presented in a journal paper, the focus is on the root-mean-square motion at the nacelle and platform level of the floaters which is relevant to assess potential problems with seasickness and effectiveness of the personnel. The second part focuses on the extreme expected motions in different reference periods to evaluate the discomfort level of the personnel and its sensitivity to the time spent on board.

Research objective: The assessment and comparison of motions of the selected FOWT concepts regarding the comfort and effectiveness of the personnel on board for two sites relevant for deployment of FOWTs.

Research objective: The evaluation of the workability of the FOWTs against the chosen limiting motion criterion and its sensitivity regarding the FOWT design, the location (platform or nacelle), the site, and the wave spectrum.

Research questions: What sea conditions are the threshold for the maintenance activity on different floater concepts and whether they are beyond the operational limits of the transfer vessels? How is the workability for the selected FOWTs during maintenance activities, and is it important to take into consideration during the design phase?

1.3. Structure of the Thesis

The thesis is structured as follows:

• Chapter 2: A concise review of the rigid body motion of floating objects, hydrostatics and hydrodynamics of the floaters, the wave-induced response of floaters in regular and irregular sea states, numerical modelling details concerning panel method and effects of mooring, and literature study of human exposure to vibration and shock are given.

• Chapter 3: A version of the paper that has been submitted to Marine Structures is given. A methodology for workability assessment on the FOWTs in the frequency domain is developed. The motion performances of the selected floaters are assessed for two different sites relevant for the deployment of FOWTs at the coast of Norway and South Korea.

• Chapter 4: Validity of the applied numerical method (linear potential theory) is investigated for the selected floaters. Extreme-expected motions of the floaters for 3 and 10 hours reference time are presented and an assessment of the discomfort level of the maintenance personnel is conducted.

• Chapter 5: Conclusions and recommendations for future work are given.

1.4. Previous Work

Human response to the occupational and long term low frequency vibrations on floating structures and vessels have been studied in several studies [5], [7], [8]. However, the first numerical study containing the study cases of reference FOWT models is performed by [5], as per the author's knowledge. The latter investigates the exposure of technicians to the motion of the floater during the maintenance of the FOWT and introduces a methodology for the workability assessment on the FOWTs in the time domain. In the referred study, the workability index of four well-known floaters; spar, semi-submersible, barge and TLP are investigated for three possible sites for FOWT installation by utilizing the load cases generated from the metocean parameters based on the design loading conditions of several codes. However, the purpose of the study was to state the importance of a new factor regarding the challenges of maintainability on the FOWTs, which was not previously considered during their design phase. Accordingly, the workability results of the chosen models were shared anonymously. Research previously performed by [5] has become a milestone approach to the maintainability & accessibility of FOWTs and has become one of the motivations of this study to investigate the comfort and effectiveness of the maintenance personnel during their time onboard the FOWT.

References

[1]   IEA, 'World Energy Outlook 2018', p. 661, 2019.

[2]   W. Musial, 'Floating Wind Turbines on the Rise', 2020. https://www.nrel.gov/news/program/2020/floating-offshore-wind-rises.html (accessed Apr. 04, 2021).

[3]   Equinor, 'Floating offshore wind in Equinor - equinor.com'. https://www.equinor.com/en/what-we-do/floating-wind.html (accessed May 17, 2021).

[4]   A. L. H. Hopstad, K. O. Ronold, and J. Slätte, 'Design Standard for Floating Wind Turbine Structures', 2013, p. 1.

[5]   M. Scheu, D. Matha, M.-A. Schwarzkopf, and A. Kolios, 'Human exposure to motion during maintenance on floating offshore wind turbines', *Ocean Engineering*, vol. 165, pp. 293–306, Oct. 2018, doi: 10.1016/j.oceaneng.2018.07.016.

[6]   DNV GL, 'Frequency domain hydrodynamic analysis of stationary vessels | Wadam', *DNV GL*. https://www.dnv.com/services/frequency-domain-hydrodynamic-analysis-of-stationary-vessels-wadam-2412 (accessed May 22, 2021).

[7]   F. Çakıcı, B. Yıldız, and A. Alkan, 'Crew Comfort Investigation for Vertical and Lateral Responses of a Container Ship', Jun. 2015. doi: 10.13140/RG.2.1.3353.0968.

[8]   H. V. C. Howarth and M. J. Griffin, 'Human exposure to low frequency horizontal motion in buildings and offshore structures: an assessment of guidance in BS 6611 and ISO 6897', p. 7, 2009.

Chapter 2

2. Theoretical Background

In this section, a concise summary of the fundamentals of this thesis is given. First, the theory of floating body motions is given within the assumption of the floater preserves its rigidness while excited by the external loads. Hydrostatics and hydrodynamics of floaters are briefly shown, then followed by the motions of the floaters in regular and irregular waves. Later, the procedure of modelling and postprocessing the results is presented, together with a brief description of the theoretical background to applied methods in the software used.. The chapter is finished with a literature review on human exposure to vibration, particularly focusing on vibrations related to motion sickness.

2.1. Linear Rigid Body Motions

Floating objects in offshore conditions are subjected to loads such as waves, current and wind that induce motion on the floating body. However, this thesis focuses on the motions of the FOWTs during the maintenance and the blades are set to the parked position while maintenance is conducted on the floating wind turbines. Therefore, in this thesis, the offshore wind turbine is assumed to be rigid and tower flexibility is neglected due to the reduced wind load.

Rigid motion can be defined as a translation of an arbitrary point on the body, followed by a rotation about that point, displayed in **Figure 2.1**. In rigid motion, the distance between 2 points always remains the same, since the rotation is assumed to be the same all along the body. So, if the motions of a point on the floating body are known either in time or in the frequency domain, the motions of another point on the body can be computed with the assumption of rotations are small enough to be linearized (<0.1 rad) [9]. The governing equation to calculate the motion at any point, S, on the body is given in **(2.1)**.

$$\begin{aligned}
\vec{S} = \ & (\eta_1 + z\eta_5 - y\eta_6)\vec{x} \\
& + (\eta_2 - z\eta_4 + x\eta_6)\vec{y} \\
& + (\eta_3 + y\eta_4 - x\eta_5)\vec{z}
\end{aligned} \tag{2.1}$$
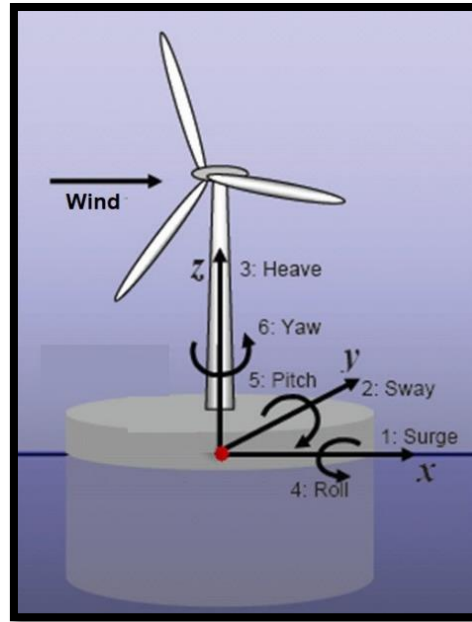
Figure 2.1: Body-fixed orthogonal coordination system of a floating offshore wind turbine and definitions of motions along/about axes [10].

In the expression above, $\vec{S}$ is the vector that represents the magnitude and the direction of the motion at an arbitrary point S on the body. $\boldsymbol{\eta_i}$ is the amplitude of a particular motion at the reference point while the index i stands for the mode of the motion (1= surge, 2= sway, 3= heave, 4= roll, 5= pitch, 6= yaw). x, y and z represent the longitudinal, transverse and vertical distance between the point S and the reference point respectively while $\vec{x}$, $\vec{y}$ and $\vec{z}$ are the unit vectors of the orthogonal axes of the coordination system.

2.2. Hydrostatics of Floaters

Hydrostatics is a branch of physics that deals with the characteristics of fluids at rest and especially with the pressure in a fluid or exerted by a fluid on an immersed body [11]. At the free surface, the fluid pressure is equal to the atmospheric pressure which is nearly always neglected in offshore hydrodynamics [9]. At any point under the water surface, a pressure occurs due to the weight of the fluid column above, which is shown in equation form for an incompressible fluid with density ρ.

$$dp/dz = -\rho g$$

(2.2)

where dp/dz represents the pressure change by depth while g is the gravitational acceleration. Due to the pressure difference between the outer and inner part of the submerged parts of the body, a net upward force occurs on the centre of buoyancy (COB), which is called buoyancy. The buoyant force acting on any body can be calculated by integrating the hydrostatic fluid pressure over the body. In the below expression F represents the buoyancy force, where ∇ stands for the submerged volume.

$$F = \rho g \nabla \tag{2.3}$$

Floating objects are assumed to rotate around a point called metacentre, M. A stable floating object's centre of gravity, G and centre of buoyancy, B must be vertically aligned while the object is floating at rest. If an external rotational moment M_H is applied to the floating body at rest, it will result in the body rotating for ϕ degrees in the direction of the applied moment. As a result of this new tilted floating condition, the new COB of the submerged body B_ϕ will shift to the more submerged side which will lead to a righting moment until the equilibrium between the external and righting moment is reached.

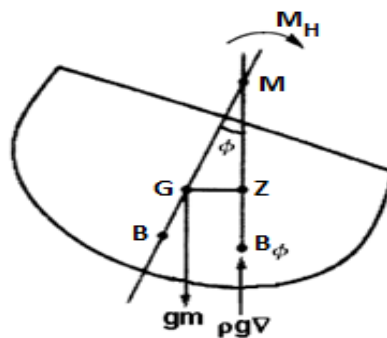**Figure 2.2:** Metacenter and metacentric height in roll

COB normally shifts both horizontally and vertically however vertical shift can be ignored in a small angle of rotation ($<10°$) [9]. As can be seen from **Figure 2.2**, the righting stability lever arm $\overline{GZ}$ can be shown for the small tilting angles as following

$$\overline{GZ} = \overline{GM} * sin\phi \tag{2.4}$$

Then righting moment M_S becomes

$$M_S = \rho g \nabla * \overline{GM} * sin\phi$$

(2.5)

To create a stable structure, a positive righting moment is needed. Therefore, positive $\overline{GM}$ is a requirement to create a stable structure for intact stability. Else, the structure will face capsizing since there won't be any righting moment. Metacentric height, $\overline{GM}$ and metacentric radius, $\overline{BM}$ can be calculated as shown in the equations below. In the expressions, $\overline{BG}$ is the distance between the centre of gravity and centre of floatation points of the body, I is the area moment of the waterplane about the relevant rotation axis.

$$\overline{GM} = \overline{BM} - \overline{BG}$$

(2.6)

$$\overline{BM} = \frac{I}{\nabla}$$

(2.7)

2.3. Hydrodynamics of Floaters

Based on Newton's second law, A rigid body's motions at any time could be expressed as:

$$\sum_{k=1}^{6} M_{jk}\ddot{\eta}_k(t) = F_j(t) \qquad j = 1, ...,6$$

(2.8)

where M_{jk} is the mass matrix of the body, $\ddot{\eta}_k$ is the body acceleration vectors for k degree of freedom and F_j is the external loads on the body. However, before getting deeper into the equation of motion, one should understand the principles of the wave-body interaction.

2.3.1. Linear Potential Theory

The linear potential theory is based on the assumption that the surrounding fluid is incompressible, inviscid, irrotational and does not have surface tension. A rigid body's interaction with linear waves is displayed in **Figure 2.3**, where S_{FS} represents the fluid's mean free surface, S_B represents the mean wetted surface of the body, S_{SB} is the surface of the seabed, Ω_0 is the mean fluid volume and V_B is the body velocity.
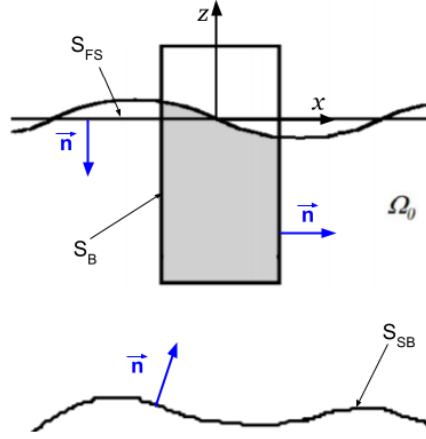
Figure 2.3: A rigid body's interaction with linear waves

So with these assumptions, a rigid body's interaction with linear waves can be described with some boundary conditions regarding potential theory:

- Continuity condition: $\qquad\qquad\nabla^2 * \phi = 0 \qquad in\ \Omega_0$ $\qquad\qquad$ **(2.9)**

- Sea bottom condition: $\qquad\qquad\dfrac{\partial \phi}{\partial n} = 0 \qquad on\ S_{SB}$ $\qquad\qquad$ **(2.10)**

- Body boundary condition: $\qquad\quad\dfrac{\partial \phi}{\partial n} = V_B * n \qquad on\ S_B$ $\qquad\qquad$ **(2.11)**

- Combined free surface condition: $\quad\dfrac{\partial^2 \phi}{\partial t^2} + g\dfrac{\partial \phi}{\partial z} = 0 \quad on\ z = 0$ $\qquad$ **(2.12)**

These are the governing equations of the linear wave-body interaction where ϕ represents the velocity potential. For linear waves, the external loads in Equation **(2.8)** can be described as the sum of the integration of the dynamic pressure over the mean wetted surface S_B and the integration of the hydrostatic pressure over the instantaneous body surface $S_{B\prime}$, shown as below:

$$F_j(t) = \int_{S_B} -\rho\frac{\partial \phi}{\partial t}\boldsymbol{n}dS + \int_{S_{B\prime}} -\rho gz\boldsymbol{n}dS \qquad j = 1,\dots,6 \qquad \textbf{(2.13)}$$

However, the motions of a floating body in linear waves may be considered as a superposition of the body response in still water and the forces on the fixed body by the incident waves due to linearity [9]. So the body-linear wave interaction could be divided into two sub-problems, as shown in **Figure 2.4** [9].

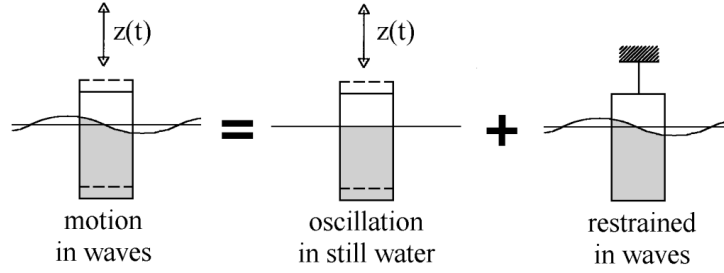**Figure 2.4:** Superposition of hydromechanical and wave loads for heave motion [9].

The first sub-problem is known as the radiation problem which considers the forced oscillation of a body in its six degrees of freedoms where there are no incident waves. The radiation problem is involved with what known as radiation potential and hydrostatic pressure. Solution of the radiation problem gives the added mass A, linear damping B and restoring forces C for that wave period. On the other hand, the second one is known as the diffraction problem which covers the interaction of the fixed-body with incident waves. The diffraction problem is involved with the potential of the incident waves and the diffraction potential. Solution of the diffraction problem gives the wave excitation loads F_{exc} as result.

So according to the superposition principle in linear theory, the velocity potential ϕ in Equation **(2.13)** could be rewritten as:

$$\phi(x,y,z,t) = \phi_0(x,y,z,t) + \phi_D(x,y,z,t) + \phi_R(x,y,z,t) \qquad \text{(2.14)}$$

where ϕ_0 represents the potential of the incident waves, ϕ_D represents the diffraction potential and ϕ_R denotes the radiation potential. With the solutions of the radiation and diffraction problems, the external loads on a body oscillating in a degree of freedom k can be rewritten as:

$$F_j(t) = \sum_{k=1}^{6} F_j^{exc}(t) - A_{jk}\ddot{\eta}_{jk}(t) - B_{jk}\dot{\eta}_{jk}(t) - C_{jk}\eta_{jk}(t) \qquad j = 1,\dots,6 \quad \text{(2.15)}$$

Then the equation of motions of a floating body in linear waves can be written as:

$$\sum_{k=1}^{6} \left[(M_{jk} + A_{jk})\ddot{\eta}_{jk}(t) + B_{jk}\dot{\eta}_{jk}(t) + C_{jk}\eta_{jk}(t) \right] = F_j^{exc}(t) \qquad j = 1,\dots,6 \quad \text{(2.16)}$$

The governing equation of motion in the frequency domain on matrix form can be written as:

$$\left(M + A(\omega)\right)\ddot{\eta} + B(\omega)\dot{\eta} + C\eta = F \tag{2.17}$$

In the above expression $A(\omega)$ and $B(\omega)$ represent the frequency-dependent added mass and potential damping matrices while $\ddot{\eta}$, $\dot{\eta}$ and η denotes the acceleration, velocity and displacement matrices of the floating body, respectively.

2.3.2. Morison's Equation

The damping term in the (2.17) only covers the potential damping but not viscous damping since in potential theory fluid is assumed to be inviscid and hence friction is neglected. However, viscous damping might be relatively larger compared to potential damping for some cases. For instance, a horizontally floating long circular cylinder would have zero dampings for the rotation around the longitudinal axis while the viscous damping may be relatively significant based on the fluid and surface properties.

The major contributor to the viscous damping is the drag force acting on the body which is not covered in the potential theory [9]. When the wave length, λ, of the incident waves are significantly larger than the diameter, D, of the floating object ($\lambda/D > 5$) [12], Morison's equation is often used to calculate the wave loads on the slender object. The non-linear drag force $F_{drag,NL}$ acting on a fixed cylinder with a diameter of D can be shown as below [12].

$$dF_{drag,NL} = \frac{1}{2}\rho C_D D |u - \dot{\eta}|(u - \dot{\eta}) \tag{2.18}$$

In the above expression, C_D represents the drag coefficient which is chosen according to the cross-section of the object, u denotes the wave-particle velocity and $\dot{\eta}$ stands for the body velocity. Hence, Equation (2.18) is a quadratic function of the relative velocity between the particle and the body. This quadratic equation can be linearized with some assumptions which the reader is referred to the reference [12] for further details. The linearized version of the drag force $F_{drag,L}$ can be written as below:

$$dF_{drag,L} = \frac{4\rho C_D D A}{3\pi}(u - \dot{\eta}) \tag{2.19}$$

where A is derived from the relative velocity u_r between fluid particles and the floating body while neglecting the phase difference;

$$u_r = u - \dot{\eta} = A cos(\omega t) \tag{2.20}$$

$$A = \frac{u - \dot{\eta}}{\cos(\omega t)} \tag{2.21}$$

The first term in the linearized drag force, Equation **(2.19)**, can be considered as viscous damping coefficient and could be written as:

$$B_{viscous} = \frac{4 \rho C_D D A}{3 \pi} \tag{2.22}$$

2.4. Wave-induced Motions of Floaters in Frequency Domain

FOWTs are expected to operate under harsh sea conditions which means they will be subjected to various types of loads such as waves, wind, current, ice, tides and marine growth. Not all of them are taken into consideration in this study since the motions of the FOWTs during their maintenance is only excited by the wave loads. Besides, only 1st order wave forces are considered as external loads and nonlinear effects -which are 2nd order wave forces- are neglected. So the governing equation motion from Equation **(2.17)** could be rewritten as:

$$(M + A(\omega))\ddot{\eta} + B(\omega)\dot{\eta} + C\eta = F^{Waves^{1st}} \tag{2.23}$$

In this section, a floating body's behaviour in regular and irregular waves in the frequency domain is investigated. First, a compact theory related to regular waves is given. Then it is followed by the floating body's response to regular waves and derivation of the transfer functions. Later, irregular waves and their parameters, and the principle of superpositioning regular waves in the frequency domain to model an irregular sea state is briefly explained. Lastly, the sub-chapter is finished with the demonstration of the spectral models -JONSWAP and Torsethaugen- that are used in the modelling of sea states.

2.4.1. Response in Regular Waves

Regular wave theory is based on the assumption that the wave is sinusoidal with constant wave amplitude ζ_a, wavelength λ, and wave period T [13]. A snapshot of a sea surface that is formed of regular waves is presented in **Figure 2.5**.
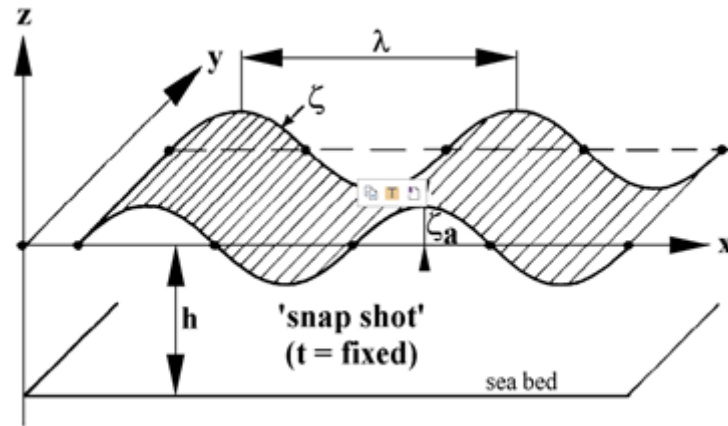
Figure 2.5: Regular wave definitions [9].

Thus the heave motion of a wave propagating in the positive x-direction could be expressed as a function of wavenumber k and a fixed time t as follows:

$$\zeta = \zeta_a \cos{(\omega t - kx)}$$
(2.24)

The wavelength λ or wavenumber k is related to wave's frequency ω by so-called dispersion relation [9]. Dispersion relation could be written for any arbitrary water depth d as follows:

$$\omega^2 = kg * \tanh{(kd)}$$
(2.25)

Equation **(2.25)** can be rewritten for deep waters as follows since $\tanh{(kd)}$ converges to 1 for $kd \geq \pi$:

$$\omega^2 = kg \quad (deep\ water)$$
(2.26)

And then the relation between waveperiod T and wavelength λ could be written as follows:

$$\lambda = \frac{g}{2\pi} * T^2 \quad (deep\ water)$$
(2.27)

The motion of a floating body in regular waves may be considered as a single linear mass-spring system. Then the harmonic part of the regular wave force can be considered as the

multiplication of the spring coefficient and the effective wave elevation. Effective wave elevation ζ^* can be written for deep water as follows:

$$
\begin{aligned}
\zeta^* &= \zeta_a e^{-kT} \cos(\omega t) \\
\dot{\zeta}^* &= -\zeta_a e^{-kT} \omega \sin(\omega t) \\
\ddot{\zeta}^* &= -\zeta_a e^{-kT} \omega^2 \cos(\omega t)
\end{aligned}
\tag{2.28}
$$

Then floating body's heave response to the regular wave excitation could be written as a function of the heave magnitude z_a as follows:

$$
\begin{aligned}
z &= z_a \cos(\omega t + \in_{z\zeta}) \\
\dot{z} &= -z_a \omega \sin(\omega t + \in_{z\zeta}) \\
\ddot{z} &= -z_a \omega^2 \cos(\omega t + \in_{z\zeta})
\end{aligned}
\tag{2.29}
$$

In above expressions $\in_{z\zeta}$ denotes the phase difference between the propagating wave and the oscillating body's response. Then the equation of motion from Equation **(2.23)** could be rewritten for the total relative heave motions between the water particles (ζ^*, $\dot{\zeta}^*$ and $\ddot{\zeta}^*$) and the heaving body (z, $\dot{z}$ and $\ddot{z}$) based on Newton's second law as follows:

$$
m\ddot{z} = a(\ddot{\zeta}^* - \ddot{z}) + b(\dot{\zeta}^* - \dot{z}) + c(\zeta^* - z)
\tag{2.30}
$$

Where m, a, b, c are relevant mass, added mass coefficient, damping coefficient and restoring coefficient of the floating body. A substitution of **(2.28)** and **(2.29)** into **(2.30)** gives an equation with two out-of-phase and two in-phase terms. One can obtain two equations with two unknowns by equating the out-of-phase and in-phase terms:

$$
\begin{aligned}
z_a\left\{\{c - (m + a)\omega^2\}\cos(\in_{z\zeta}) - \{b\omega\}\sin(\in_{z\zeta})\right\} &= \zeta_a e^{-kT}\{c - a\omega^2\} \\
z_a\left\{\{c - (m + a)\omega^2\}\sin(\in_{z\zeta}) - \{b\omega\}\cos(\in_{z\zeta})\right\} &= \zeta_a e^{-kT}\{b\omega\}
\end{aligned}
\tag{2.31}
$$

This could be considered a complex vector. Then magnitude which is also called response amplitude operator (RAO) could be found by adding the squares of these two equations:

$$
RAO = \frac{z_a}{\zeta_a} = e^{-kT}\sqrt{\frac{\{c - a\omega^2\}^2 + \{b\omega\}^2}{\{c - (m + a)\omega^2\}^2 + \{b\omega^2\}}}
\tag{2.32}
$$

And elimination of $z_a/\zeta_a e^{-kT}$ would give the phase shift:

$$\epsilon_{z\zeta} = \arctan\left\{\frac{-mb\omega^3}{\{c - a\omega^2\}\{c - (m + a)\omega^2\} + \{b\omega\}^2}\right\} \quad where: 0 \leq \epsilon_{z\zeta} \leq 2\pi \quad \textbf{(2.33)}$$

2.4.2. Response in Irregular Waves

Ocean waves are often not regular and it is also referred to as random or confused sea [14]. One rarely observes a pattern of unidirectional regular sinusoidal waves in the open seas, but often observes irregular sea with a mixture of waves with different length, height and directions. However, this mixture of waves with different parameters may be considered as a combination of regular waves with different heights, steepnesses and phase angles, which is also known as the superposition principle. An irregular wave can be considered as a composition of some regular waves with different amplitude ζ_i, wavelength λ_i, and phase angle ϵ_i. In **Figure 2.6**, an irregular wave is demonstrated as a composition of three simple sine waves.
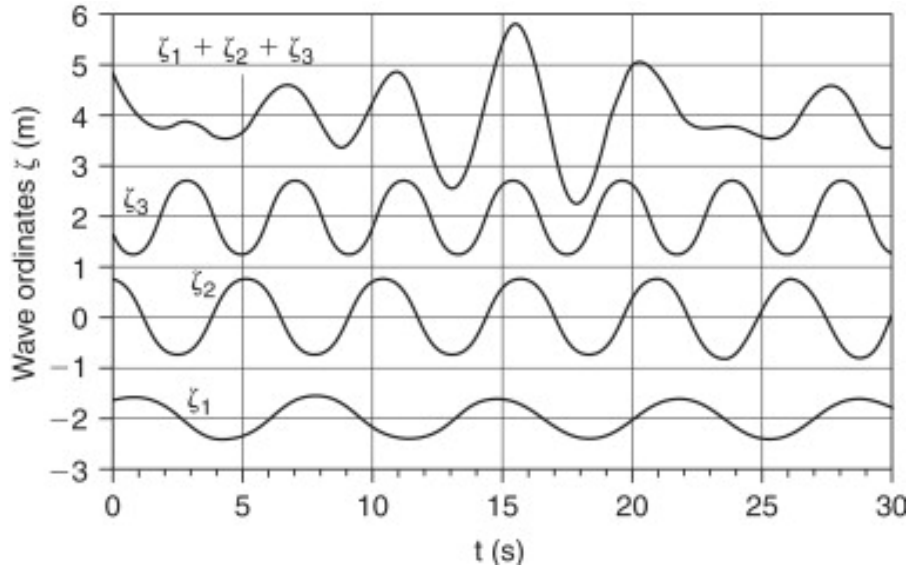
Figure 2.6: Superposition principle of three simple sine waves to represent an irregular wave [14].

The wave elevation of a long-crested irregular sea as a function of time could be written as the sum of N regular waves in the frequency domain as follows:

$$\zeta(t) = \sum_{n=1}^{N} \zeta_{a_n} \cos(k_n x - \omega_n + \epsilon_n) \quad \textbf{(2.34)}$$

Where ζ_{a_n} is the wave amplitude, ω_n is the angular frequency, k_n is the wavenumber and ϵ_n is the phase angle of each component, n. Then the wave amplitude ζ_{a_n} can be expressed as a continuous energy distribution function for each frequency, the so-called wave spectrum. The

reader is referred to reference [9] for the derivation of the wave spectrum. The wave energy spectrum of an irregular sea for each regular wave component, n, could be written as follows:

$$S_\zeta(\omega_n) * d\omega = \frac{1}{2}\zeta_{a_n}^2 \tag{2.35}$$

Similar to this, by substituting the heave motion amplitude from Equation **(2.29)** into Equation **(2.33)**, one can find the energy spectrum of the heave motion as a function of frequency as follows:

$$S_z(\omega) * d\omega = \frac{1}{2}z_a^2(\omega) \tag{2.36}$$

Equation **(2.36)** represents the energy spectrum of the heave motion only and could be rewritten for 6 degrees of motion as follows:

$$S_k(\omega) * d\omega = \frac{1}{2}\eta_{a_k}^2(\omega) \tag{2.37}$$

Where index k represents any degree of motion and η_a represents the amplitude of the motion. Then, the energy spectrum could be rewritten in terms of RAO by substituting the frequency-dependent amplitude term $\eta_{a_k}(\omega)$ from Equation **(2.37)** with Equation **(2.32)**:

$$S_k(\omega) * d\omega = \left|\frac{\eta_{a_k}}{\zeta_a}(\omega)\right|^2 * \frac{1}{2}\zeta_a(\omega) \tag{2.38}$$

Then, by substituting Equation **(2.35)** into Equation **(2.38)**, one can find the response spectrum of any degree of motion k, as a function of RAO and the wave spectrum in the frequency domain.

$$S_k(\omega) = \left|\frac{\eta_{a_k}}{\zeta_a}(\omega)\right|^2 * S_\zeta(\omega) * d\omega \tag{2.39}$$

Since it is a continuous function, the moments of the response spectrum can be found by:

$$m_{nz} = \int_0^\infty S_k(\omega) * \omega^n * d\omega \tag{2.40}$$

Where n=1,2,3 provides the area moment, the first moment and the moment of inertia of the spectral curve. The average zero-crossing period T_2, which is an important characteristic to estimate the statistical motions in a reference time, could be written as follows:

$$T_2 = 2\pi * \sqrt{\frac{m_0}{m_2}}$$

(2.41)

Estimation of the statistical motions such as root mean square and expected extreme motions in a reference time T, could be written as follows:

$$r.m.s. = \sqrt{m_0}$$

$$E[n_{max,T}] = \sqrt{m_0} * \sqrt{2 \ln\left(\frac{T}{T_2}\right)}$$

(2.42)

2.4.2.1. Spectral Models

Characteristic parameters for an irregular sea such as a significant wave height, period, and direction of progress can be estimated with careful observation with the assumption of the sea surface is stationary for a duration of 20 minutes to 2-6 hours [14]. The significant wave height H_s and peak period T_p are commonly used parameters to define a stationary sea state to model the ocean conditions. Waves in the oceans are mainly formed by the wind and therefore, the wave characteristics of each location are unique. Accordingly, spectral models that are developed over the years are relevant for specific locations. For instance, one of the spectral models, JONSWAP, that is utilized in this thesis is assumed to be especially suitable for the North Sea and it is a reasonable model for wind-generated sea when [15]:

$$3.6\sqrt{H_s} < T_p < 5\sqrt{H_s}$$

(2.43)

The following parameters of the JONSWAP model define a wave spectrum as a function of H_s and T_p [16]:

- Non-dimensional peak shape parameter; $\gamma = 3.3$

- Spectral width parameters; $\sigma_a = 0.07$, $\sigma_b = 0.09$

- Normalization factor; $A_\gamma = 1 - 0.287\ln(\gamma)$

- Spectral peak frequency; $\omega_p = 2\pi/T_p$

Then JONSWAP spectrum S_J, can be represented as a function of angular frequency, ω;

$$S_J(\omega) = \frac{5}{16} * H_s^2 \omega_p^4 * \omega^{-5} * \exp\left[-\frac{5}{4}\left(\frac{\omega}{\omega_p}\right)^2\right] * A_\gamma * \gamma^{\exp\left[-0.5\left(\frac{\omega-\omega_p}{\sigma\omega_p}\right)^2\right]} \tag{2.44}$$

On the other hand, the Torsethaugen spectrum is also used within this thesis to model sea states. The Torsethaugen spectrum, which is commonly used for design purposes at the Norwegian Continental Shelf, is established by fitting two JONSWAP shaped peaks to average measured spectra from Norwegian Continental Shelf [17]. One should note that the Torsethaugen spectrum is a double-peaked spectrum that is composed of swell and wind sea components respectively for low frequency and high-frequency range. The Torsethaugen spectrum is a reasonable model for the North Sea when [17]:

$$\begin{aligned} H_s &\leq 11 \\ 3 &\leq T_p \leq 20 \end{aligned} \tag{2.45}$$

The parameters of the Torsethaugen spectrum is based on the input H_s and T_p values. According to the input values, different parameters are recommended whether the sea is wind or swell dominated. The reader is referred to reference [17] for for further details about the derivation of the Torsethaugen spectrum.

Figure 2.7 show the same irregular sea state $(H_s = 1m$ and $T_p = 12.6s)$ modelled with both JONSWAP and the Torsethaugen spectrums. The variation of the wave spectral density based on the spectral model used is clear. .
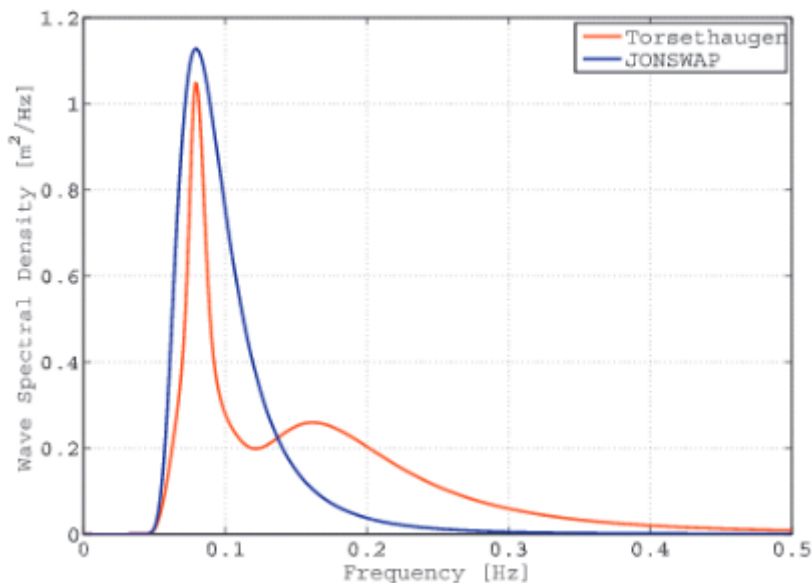
Figure 2.7: Wave spectral density of an irregular sea state ($H_s = 1m$ and $T_p = 12.6s$) modelled by using the JONSWAP and the Torsethaugen spectral models [18].

2.5. Modelling

The software programs used for modelling of the FOWT concepts in this study are presented in this section. Later in this section, available potential theory application methods such as strip theory and panel method are presented. Lastly, the section is finished with the details of the hydrodynamic models of the FOWT concepts that are analyzed.

First, the geometries of the FOWT concepts that are analyzed, are modelled and meshed either with GeniE or Rhinoceros. Then the created panel models are exported as .FEM files with their fixed coordinate system. Later, these 3D panel models are imported to HydroD to build a valid hydrodynamic model by augmenting the panel model with mass matrix and linear damping matrix. Then, motion response simulation is run in the frequency domain by utilizing Wadam code through HydroD interface. RAOs and phase angles of each degree of freedom are exported as 5S.out and 5S.4 files. Then these RAOs and phase angles of each degree of freedom are combined in MATLAB with metocean data to estimate the statistical motions of the study cases in irregular sea states for a determined duration. **Figure 2.8** shows the workflow of for the modelling procedure for the numerical study conducted within this thesis.
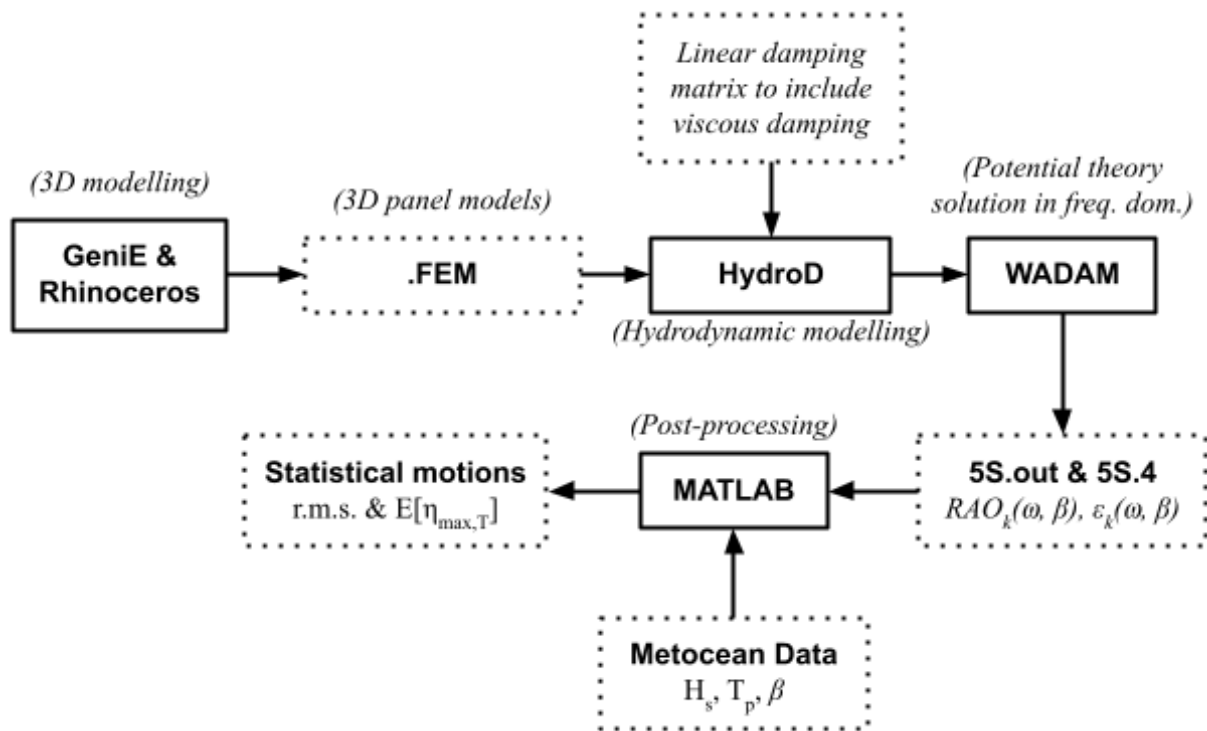
Figure 2.8: Workflow of the analysis conducted within the thesis.

2.5.1. Strip Theory

Strip theory is a method to compute the forces and motions of a 3-D floating body based on the solutions derived from the 2-D potential theory [9]. In strip theory, the floating body is assumed to be made up of a finite number of thin slices where each slice is considered to be a segment of an infinitely long floating cylinder, depicted in **Figure 2.9**. Hydrodynamic properties (added mass, damping and stiffness) of each slice is assumed to contribute to the coefficients for the complete hull in the equation of motion, and simimlarlyfor the wave loads experienced by the hull consists of the contributions from all the slices [19].

Figure 2.9: Representation of underwater hull section shapes by an infinite cylinder [19].

Strip theory is applicable if;

- The floating body has no or low forward speed

- The floating body is slender and has low longitudinal geometrical variation ($L/B \geq 3$)

- The frequency of encounter is high

However, floating offshore wind turbines are relatively wide structures and may be subjected to low-frequency oscillations. Therefore, strip theory is not applied in this thesis.
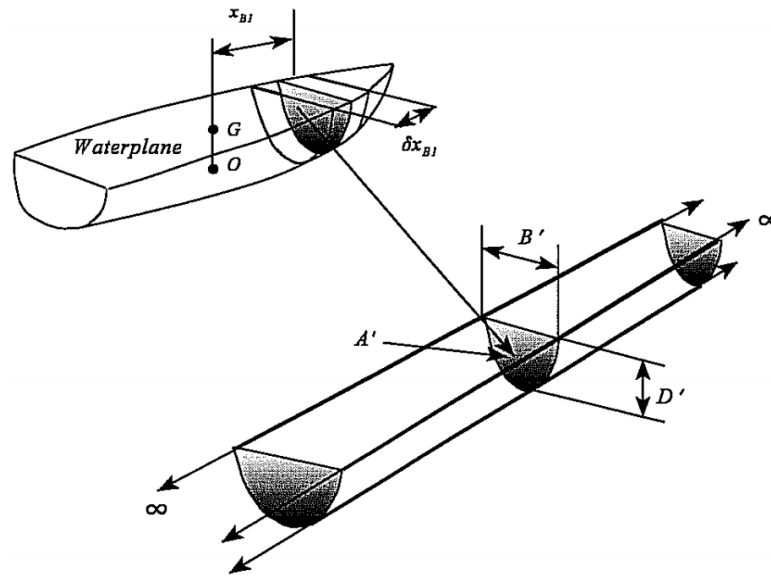
2.5.2. Panel Method

Panel method is a numerical method based on the potential flow theory to calculate the flow around any floating body using the principle of Green's integral theorem [20]. It is an adequate simplification for the vast majority of the bottom-fixed and floating structures with zero mean forward speed [9].

The method reduces the 3-D volume problem into the 2-D surface problem by dividing the body into N amount of small panels. Each panel of the body is defined by the simple nodes as can be seen from **Figure 2.10**. By using the boundary conditions which will be presented later in this chapter, velocity potentials along the body can be found as well as the frequency-dependent hydrodynamic coefficients. Wave-induced hydrodynamic loads on the floating body and its corresponding motions can be computed by the panel method [9]. The panel method applies to

almost any type of body except slender structures such as risers or tethers since the method is based on the potential theory and the effect of flow separation is neglected.
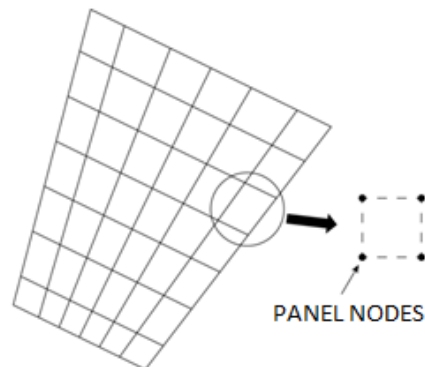

Figure 2.10: Illustration of an arbitrary panel geometry; shown here is a surface of what could be a three-dimensional object such as an entire aeroplane [21].

2.5.3. Hydrodynamic Model

A 3D panel model is created for each study case based on the definition reports of each floater [22]-[24]   of which details will later be explained in Paper I: Analysis of spar and semi-submersible floating wind concepts with respect to human exposure to motion during maintenance operations. Panel models of two study cases, OC3-Hywind and CSC-Semisubmersible, are formed by utilizing GeniE which is a 3D modelling and structural analysis tool for fixed or floating structures by DNV [25]. On the other hand the third FOWT concept, the WindFloat model is created by using Rhinoceros due to the model's geometrical complexity, which is a commonly used 3D modelling tool for industrial designers. Since the floating platform is assumed to remain in its undisplaced position according to frequency domain analysis in potential theory, it was sufficient to model only the geometries below the SWL.

Each panel is subjected to "dummy" hydrodynamic pressure to define a normal vector of each panel in the software [26]. To check the mesh quality and the accuracy of the results depending on mesh size, one FOWT concept is modelled 3 times with different mesh size. Based on the comparison of the results, in the end, the largest mesh size was chosen to decrease simulation time, since the effect of mesh size on the hydrodynamic properties were negligible. The 3D panel model created for OC3-Hywind in GeniE can be seen in **Figure 2.11**.
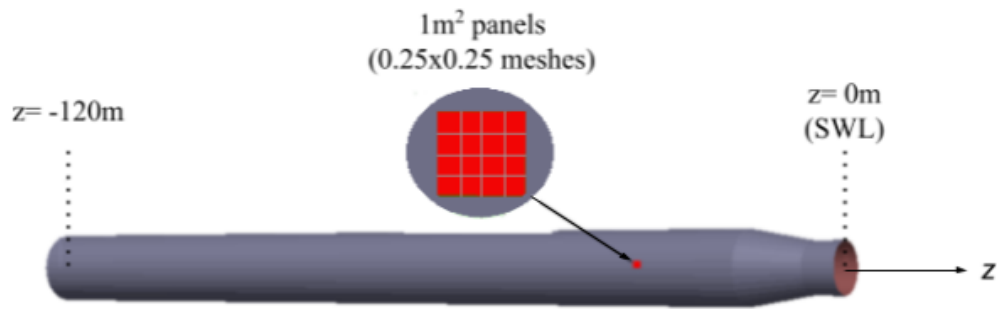
Figure 2.11: Panel mesh of OC3-Hywind model.

The OC3-Hywind panel model consists of ≈4000 rectangular panels while CSC-Semisubmersible's model is formed with ≈2000 panels. The WindFloat panel model has ≈9000 panels due to the complexity of the geometry. The largest panel and mesh size are set to 1x1 m^2 and 0.25x0.25 m^2 respectively for all models.

HydroD is used as an interface to Wadam code to get the hydrodynamic properties of the study cases and solve the problem of radiation and diffraction of linear potential theory [26], [27]. The Wadam code is capable of performing frequency domain analysis on Panel and Morison models. The 3-D panel method is used to calculate velocity potentials and hydrodynamic coefficients around the wet body.

HydroD is a stability module essentially; however, it also provides an interface to build the hydrodynamic model and its environment that are going to be used in the frequency domain analysis by WADAM. First, the environmental conditions of the simulation are set as below:

- Regular wave frequency set, [0-0.5] Hz

- Wave headings direction set, only head wave (0°)

- Water density, $\rho = 1025 kg/m^3$

- Water kinematic viscosity, $v = 1.19e^{-6} \, m^2/s$

- Water depth, $z = -320 \, m$

The wave frequency range is set to 0-0.5 Hz with smaller steps between 0-0.05 Hz to increase the accuracy of outputs around natural frequencies. Bodies' motions on the dominant wave direction and the direction of the defined DOFs are investigated and presented in **Chapter 4.2**.

To calculate the motions of the floaters in the dominant wave direction, wave directions are set to only 0° and bodies are rotated around the z-axis of the coordination system.

Then, each panel is model is augmented with the relevant mass matrix as if they are in their operating condition (including the mass of the tower, hub, blades and ballast) according to its rotational arrangement. Also, chosen three study cases are station kept with catenary mooring lines. Therefore, the additional restoring matrix is added to include the effect of mooring line stiffness in the frequency domain. Lastly, the damping term that is provided by the potential theory based solution in WADAM only includes the radiation potential but not viscous terms. Therefore, to include the effects of the viscous damping in the response analyses of each floater, the potential damping matrix from Equation **(2.17)** is augmented with a linearized damping matrix that is based on experimental studies [22]–[24].

2.6. Human Exposure to vibration

A vibration signal may be described by its measured amplitude changing throughout a reference time or amplitude of vibration versus the frequency spectrum of the source. Human exposure to vibration-induced motions are classified into 3 groups depending on the motion characteristics such as frequency and magnitude [28];

- Hand-transmitted vibration

- Whole-body vibration

- Motion sickness (low-frequency motions)

Hand-transmitted vibration is caused by localized vibrations usually due to usage of tools with high-frequency (8 Hz-1000 Hz) operating conditions such as drilling machine, joy-stick etc. [28].

So-called "Whole-body vibration" is the vibration that affects the whole body and can affect the performance, health and comfort of the exposed person based on the exposure time. Whole-body vibration is relevant in the frequency range of 1-20 Hz and is usually transmitted by the seats attached to the vehicle or the floor [28].

On the other hand, motion sickness is a complex syndrome that occurs due to the difference between actual and perceived motion [29]. The common characteristic of all the motions which induce motion sickness seems to be a repetitive or angular acceleration of the head. Motion sickness is relevant when an individual is exposed to low-frequency motions under 1 Hz. Consequently, motion sickness will be the vibration type, which is relevant in this study, since global motions experienced on FOWTs are generally under 1 Hz and natural frequencies of all global motion modes of the reference models are below 0.5 Hz [5].

Due to the complexity of the human body, frequency range and amplitude of the vibration are not the most ideal way to evaluate the effect of the exposure to vibration in an analysis where results are derived with short term statistics. Accordingly, some international standards define the limit of exposure to vibration in terms of root mean square (R.M.S) of the acceleration signal of the vibration source, in this case the floating platform. Nordforsk (1987) is a publication that presents limiting motion exposure criteria for different kinds of work conducted by humans on vessels [30], as listed in **Table 1**.

Table 1: Limiting criteria regarding accelerations and rotation [30].

Description	Vertical acceleration (R.M.S.)	Lateral acceleration (R.M.S.)	Rotation (R.M.S.)
Light manual work	0.20g	0.10g	$6.0°$
Heavy manual work	0.15g	0.07g	$4.0°$
Intellectual work	0.10g	0.05g	$3.0°$
Transit passenger	0.05g	0.04g	$2.5°$
Cruise liner	0.02g	0.03g	$2.0°$

.

Other than durational exposures to vibration, instantaneous peaks of the vibration could be uncomfortable for humans as well. For instance, ISO-2631/1 states reference values for grading the human comfort concerning the magnitude of exposure to instantaneous accelerations [31], which is listed in **Table 2**. The standard also states that the reactions of humans vary based on the individual's expectations about trip duration and the type of activities that are expected to be accomplished during the trip [31].

Table 2: Comfort reactions to instantaneous vibration magnitude [31].

Description	Vertical acceleration (R.M.S.)
$a < 0.315 \text{ m/s}^2$	Not uncomfortable
$0.315 < a < 0.630 \text{ m/s}^2$	A little uncomfortable
$0.5 < a < 1 \text{ m/s}^2$	Fairly uncomfortable
$0.8 < a < 1.6 \text{ m/s}^2$	Uncomfortable
$1.25 < a < 2.5 \text{ m/s}^2$	Very uncomfortable
$a > 2 \text{ m/s}^2$	Extremely ncomfortable

References

[5] M. Scheu, D. Matha, M.-A. Schwarzkopf, and A. Kolios, 'Human exposure to motion during maintenance on floating offshore wind turbines', *Ocean Engineering*, vol. 165, pp. 293–306, Oct. 2018, doi: 10.1016/j.oceaneng.2018.07.016.

[9] J. M. J. Journée and W. W. Massie, *Offshore Hydromechanics*. 2001.

[10] J. Chen and C. Li, 'Design Optimization and Coupled Dynamics Analysis of an Offshore Wind Turbine with a Single Swivel Connected Tether', *Energies*, vol. 13, no. 14, p. 3526, Jul. 2020, doi: 10.3390/en13143526.

[11] Britannica, 'Hydrostatics | physics', *Encyclopedia Britannica*, 2009. https://www.britannica.com/science/hydrostatics (accessed May 26, 2021).

[12] O. M. Faltinsen, *Sea loads on ships and offshore structures*. 1990.

[13] A. Sayigh, *Comprehensive Renewable Energy*. 2012.

[14] A. F. Molland, *The Maritime Engineering Reference Book*. 2008. [Online]. Available: https://doi.org/10.1016/B978-0-7506-8987-8.00013-5.

[15] DNV GL, 'DNV-RP-C205: Environmental Conditions and Environmental Loads', *DNV-RP-C205: Environmental Conditions and Environmental Loads*, p. 124, 2010.

[16] DNV GL, 'DNVGL-CG-0130 Wave loads', *DNVGL-CG-0130 Wave loads*, p. 84, 2018.

[17] K. Torsethaugen, 'A two peak wave spectral model', 1993, p. 9.

[18] J. Mas-Soler, A. N. Simos, and E. A. Tannuri, 'Estimating on-site wave spectra from the motions of a semi-submersible platform: An assessment based on model scale results', *Ocean Engineering*, vol. 153, pp. 154–172, Apr. 2018, doi: 10.1016/j.oceaneng.2018.01.069.

[19] Lloyd, *Seakeeping: Ship behaviour in rough weather*. 1989.

[20] C. C. Ksiing and Z. Huang, 'COMPARISON OF THE STRIP THEORY AND THE PANEL METHOD IN COMPUTING SHIP MOTION WITH FORWARD SPEED', p. 8, 1991.

[21] J. Liburdy, *Intermediate Fluid Mechanics*. Oregon State University, 2020.

[22] J. Jonkman, 'Definition of the Floating System for Phase IV of OC3', NREL/TP-500-47535, 979456, May 2010. doi: 10.2172/979456.

[23] C. Luan, Z. Gao, and T. Moan, 'Design and analysis for a steel braceless semi-submersible hull for supporting a 5-MW horizontal axis wind turbine', p. 296, 2016.

[24] D. Roddier, A. Aubault, A. Peiffer, and J. Weinstein, 'A GENERIC 5 MW WINDFLOAT FOR NUMERICAL TOOL VALIDATION & COMPARISON AGAINST A GENERIC SPAR', p. 9, 2011.

[25] DNV GL, 'GeniE User Manual'. DNV GL, 2016.

[26] DNV GL, 'HydroD User Manual'. 2014.

[27] DNV GL, 'Wadam User Manual'. DNV GL, 2014.

[28] N. J. Mansfield, *Human response to vibration*. Boca Raton, FL: CRC Press, 2005. Accessed: Apr. 18, 2021. [Online]. Available: http://site.ebrary.com/id/10162776

[29] V. Takov and P. Tadi, 'Motion Sickness', in *StatPearls*, Treasure Island (FL): StatPearls Publishing, 2021. Accessed: Jun. 03, 2021. [Online]. Available: http://www.ncbi.nlm.nih.gov/books/NBK539706/

[30] NORDFORSK, *Assessment of Ship Performance in a Seaway: The Nordic Co-operative Project: 'Seakeeping Performance of Ships'*. Copenhagen, 1987.

[31] ISO, 'ISO 2631-1: Mechanical vibration and shock'. 1997.

Chapter 3

3. Paper I: Analysis of spar and semi-submersible floating wind concepts with respect to human exposure to motion during maintenance operations

A similar version of the draft of the paper that has been submitted to Marine Structures journal is presented in this chapter. The aim of this study is to investigate the comfort of the technicians on the floating offshore wind turbines during their maintenance. Three floaters, OC3-Hywind, CSC-Semisubmersible and the WindFloat are chosen as the reference models of which configurations are covered in the paper. Dynamic properties of the chosen floaters are investigated. Statistical motions of the floaters in 3 hour reference duration are estimated for two sets of approximately 500 load cases which are deriven from the hindcast data of two relevant locations for floating offshore wind turbine deployment. Estimated motions of the floaters are assessed against a chosen limiting motion criteria regarding the health and effectiveness of humans. Load cases that have one degree of motion exceeding the criteria are considered as unworkable. Workability index at two chosen sites which is the ratio of workable cases to all load cases is presented for all reference models.

Analysis of spar and semi-submersible floating wind concepts with respect to human exposure to motion during maintenance operations

Mert Kaptan[a], Bjørn Skaare[a, b, *], Zhiyu Jiang[c], Muk Chen Ong[a]

[a] Department of Mechanical and Structural Engineering and Materials Science, University of Stavanger, Stavanger, Norway

[b] Equinor ASA, Stavanger, Norway

[c] Department of Engineering Sciences, University of Agder, Grimstad, Norway

Abstract

Floating offshore wind turbines (FOWTs) are expected to experience onsite maintenances and inspections during their lifetimes. To carry out offshore maintenance activities, a crew will be transferred to a FOWT and spend several hours on board. A challenge may arise if the motions of a floating platform affect the crew's comfort level and further jeopardise their work performance or even health. To address this challenge, this paper analyses the motion characteristics and dynamic properties of a spar and two semi-submersible FOWTs, all exhibiting very different motion characteristics. The impact of the platform motions and accelerations on the workability of the FOWTs are investigated. We carry out hydrodynamic analysis in a potential-flow software for the FOWTs and estimate the relevant short-term root-mean-square values for relevant motions and accelerations of the parked FOWTs in the frequency domain. Hindcast data for two representative sites in Norway and South Korea are selected, and both single peaked and double peaked wave spectra are considered. Using the limiting motion response criteria from a NORDFORSK study, we calculate the workability index of the FOWTs for the two locations. It is found that both the spar and the semi-submersible floating wind concepts fulfil the limiting criteria for significant wave heights up to the maximum known significant wave height for crew transfers to FOWTs. The present study contributes to a better understanding of FOWTs during the maintenance phase.

Keywords: Offshore Wind; Floating Platforms; Response Amplitude Operator; Seasickness; Workability

1. Introduction

A water depth of 60 meters is considered as a cut-off level for bottom-fixed structures and the entry point of the floating platforms in the offshore wind industry due to economic reasons [1]. According to Musial [1], almost 80% of the world's offshore wind resource potential is currently profitable only for floating offshore wind turbines (FOWTs).

Some of the floating platform concepts such as spar buoys, semi-submersibles and tension-leg-platforms are well-proven concepts after years of successful operation in the oil and gas industry

[2]. Spar buoys are ballast-stabilised simple structures with inherently high stability with a large draft which decreases their deployments in relatively shallow waters. Semi-submersibles are complex free-surface stabilised structures with a relatively small draft which provides high site flexibility. Tension leg platforms are mooring line-stabilised structures with low weight that are potentially sensitive to the mooring and anchoring systems and involve a complex installation.

The 2.3 MW spar buoy concept Hywind Demo was the first full-scale FOWT in the world when installed off the West coast of Norway in 2009 [3], while the 2 MW WindFloat 1 was the first full-scale semi-submersible wind turbine when installed off the coast of Portugal in 2011 [4]. Among the 15 floating wind turbines that are currently online in the world [5], there are 8 spar buoys, 5 semi-submersibles and 2 barges with damping pool. The floating wind industry is still at an early stage, but a rapid development is expected over the next 5 years. 17 floating wind projects are under development with an overall installed capacity above 2 GW between 2021 and 2026, with semi-submersible floaters as the dominating concept [5].

Operation and maintenance will become increasingly important as floating wind projects move from demonstration and pre-commercial stages to commercial stages. Even though humans are not needed in the operation of FOWTs on a daily basis, they are still required to be on board to perform corrective, condition-based or calendar-based maintenances. By today, access to the offshore wind turbines is conducted with 3 main transport types; *(i) Crew Transport Vessel (CTV)*, *(ii) Service Operations Vessel (SOV)* and *(iii) Helicopter*, based on the scale of the operation, i.e., how far a platform is located from shore and forecasted sea and weather conditions. CTVs and SOVs are mainly restricted by the sea conditions, while visibility, wind speed and motions of the floater are the main concerns for transportation with a helicopter. SOVs are larger and better-equipped vessels compared to CTVs.

Figure 1 shows that a maintenance operation on a FOWT may be considered as a combined problem of accessibility and maintainability. The operation begins with the transfer of the technicians and required equipment to the platform. It is important to maintain the well-being of the personnel onboard during the transfer. Therefore, most vessels are equipped with individual suspension seats to minimise the travel fatigue and stress caused by the vessel motion [6]. After arrival at the platform, the vessel must be station-kept and a safe access between the vessel and the platform needs to be maintained. For that purpose, some vessels are equipped with station keeping systems such as dynamic positioning or a gripping system which improves access to the turbine ladder [7]. Motion compensated gangway systems are often applied to provide safe access to the platform. Access to the platform is mainly constrained by the sea conditions and relevant operational limits of the transfer vehicle and the equipment used in this operation while the duration is related with the distance to the platform and the vessel and equipment properties. Operational limits (OP_{lim}) of the some SOVs may reach up to significant wave height H_s of 4.5m while gangways usually operate H_s below 3m. For further information about the operational limits of the commercial transfer vessels, gangways and dynamic positioning systems, reader is referred to the reference [6]. However, this study particularly focuses on the maintainability of the FOWTs and maintenance activity conducted onboard with its constraints.

	Offshore transfer	Landing of the boat	Crew transfer	Onboard maint.	End of the task
Description	Transfer of the technicians and the equipment from the port to the asset.	Station keeping of the boat and arranging the gateway between the vessel and the asset.	Boarding of the crew and the equipment to the platform through the gateway.	Maintenance activity conducted on the asset; fault-finding, inspection, component exchange, service, etc.	Transfer of the crew and the equipment to the boat and then to the port.
Constraints	OP_{lim} of the transfer vessel.	OP_{lim} of the dynamic positioning and the gangway system.	OP_{lim} of the dynamic positioning and the gangway system.	Response of the FOWT which may be jeopardising the effectiveness and the health of the personnel.	
Duration	Depends on the distance between the port and the asset. ($\cong$2h for 50 km)	Depends on the qualifications of the dynamic positioning and gangway system.	Depends on the equipment needed on board and the type of the gangway system.	Depends on the maintenance task and whether a crane is required. ($\cong$10h for inspection)	

Figure 1. Flow chart with the different stages of a regular maintenance activity performed on an FOWT from start (left) to the end (right) with the descriptions (top), constraints (middle) and approximate durations (bottom) of each stage. The focus of this study; onboard maintenance (blue) is highlighted.

Besides accessibility, maintainability of FOWTs is also important to avoid longer downtime, re-scheduling of the maintenance operation and potential extra operation and maintenance costs. The maintainability of FOWTs is also dependent on the workability of maintenance personnel. When it is considered that a typical workday offshore counts 12 hours which approximately consists of 10 hours spent on the platform and 2 hours spent on the transfer vessel, comfort and effectiveness of the maintenance personnel onboard the FOWT becomes an important matter to finish the maintenance activity within a pre-decided weather window [8]. Therefore, the motion characteristics of the FOWTs and the exposure of maintenance personnel to their motions are important to achieve high maintainability for the asset.

The motions of the FOWTs may be considered as a vibration signal to investigate the exposure of the maintenance personnel. The signal could be defined by its measured amplitude throughout a period or amplitude of vibration versus the frequency spectrum of the source which is the floater in this case. Based on the frequency range of the excitation vibration and its effect on humans, human exposure to vibration may be categorised under two categories [9]. The first category is called whole-body vibration, which defines the vibration within a frequency range from 0.5 to 80 Hz that affects the whole body. It is common to experience such vibration while travelling in a car, bus, train etc. On the other hand, the second category is referred to as hand-arm vibration, which expresses the vibration that affects only the part of the body in contact with the vibration source, typically in a frequency range of 6.5 to 1250 Hz. This type of vibration may be experienced while using a drilling machine or while driving a car by transmitting from the device to the human body through hands and arms. An FOWT will typically be in parked condition during maintenance activities and the dynamic response is dominated by wave excitations. Since both the natural frequencies of FOWTs and the wave frequency range are usually well below 1 Hz, only whole-body vibration is considered relevant and investigated in this study.

Typical frequency ranges and the symptoms relevant to the magnitude of the vibration has been discussed by [10] and is illustrated in Figure 2. Exposure of motion sickness and whole-body vibration for a certain time could cause health problems, that would endanger the health and safety of the maintenance personnel during their work on the platform, such as dizziness, nausea and vision loss [9]. Sufficient magnitude of hand-transmitted vibration could also cause health issues such as muscle and joint disorders if it occurs long enough [10]. However, this study particularly focuses on the motions of FOWT and its possible effects on the personnel.
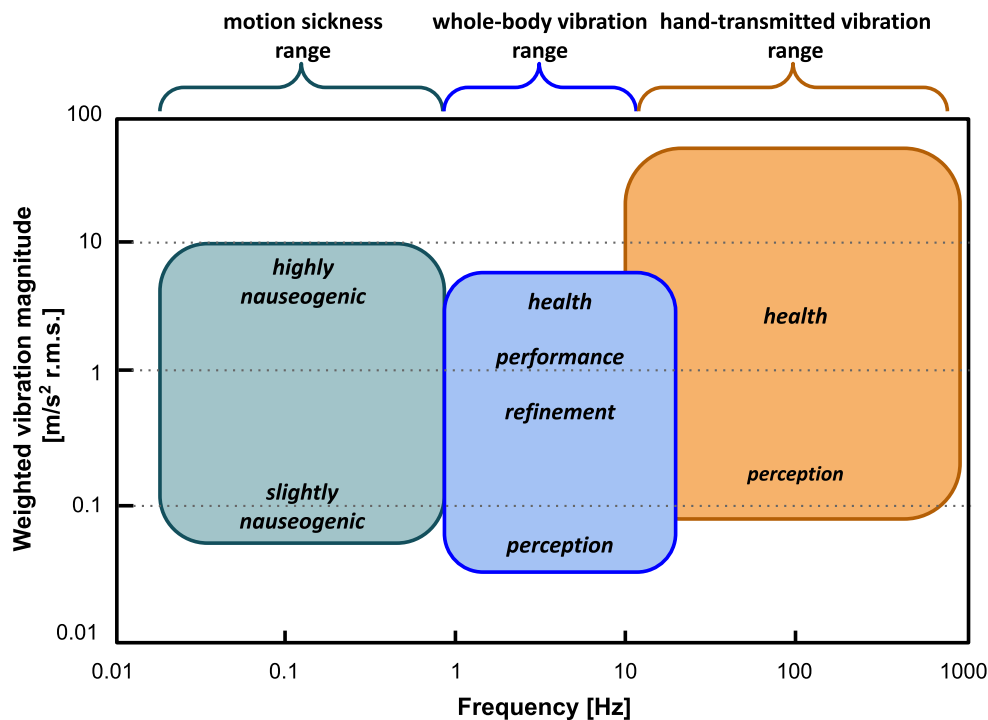

Figure 2. Typical frequency ranges and magnitudes of interest for the study of motion sickness (green), whole body vibration (blue), and hand-transmitted vibration (orange).

The frequency range and amplitude of the vibration are not the most ideal way to evaluate human exposure to vibration considering the complexity of the human body. Accordingly, most international standards define the limit of human exposure to vibration in terms of root mean square (RMS) values of motions of the excitation source, which is the floating platform in this case.

Human exposure to motion during maintenance of floating offshore wind turbines is previously studied [8] by response analyses in the time domain for four different floater concepts. In the study, spar, semi-submersible, barge and tension leg platform concepts were simulated with load cases generated from metocean parameters based on the design loading conditions at different locations. The concept of using a workability index as a measure for the workable time relative to all available time below a given significant wave height was introduced based on relevant motion and acceleration limiting criteria from the NORDFORSK study [11]. The workability index was calculated for all four floater concepts, but the results for the different concepts were anonymised.

The purpose of this paper is to analyse and compare the inherent dynamic properties of two of the dominant FOWT concepts – the spar buoy and the semi-submersible – with respect to

important parameters for human exposure, such as floater pitch motion, horizontal and vertical acceleration at both the platform and nacelle level, where maintenance work is carried out. Further, analyses are carried out in the frequency domain to compare

- The responses relevant for human exposure based on generic sea states using both the JONSWAP (Joint North Sea Wave Project) [12] and Torsethaugen wave spectra [13].
- The workability index for two relevant locations for future deployment of floating wind – one location at the coast of Norway and one location at the coast of South Korea - based on random load cases from hindcast data with good correlation with the long-term distributions for waves and directions and using both the JONSWAP and Torsethaugen wave spectra.

2. Methodology

The methodology developed for numerical study of the human comfort on an FOWT is given in this section. First, the frequency-domain approach is presented including the assumptions made and modelling/simulation tools used. Second, short-term statistics is provided for estimating floater's responses in irregular sea conditions, followed by the sets of load cases that are generated from the hindcast data of two sites relevant to FOWT deployment. Then, the derivation and choice of adequate limiting motion criterion regarding the exposure of humans to vibration is explained. Last, the definition and calculation of the workability index is presented.

2.1. Frequency-domain approach

During offshore access and maintenance operations, FOWTs are typically parked, and their motions are mainly caused by the wave-induced rigid body motion of the platform [14]. Therefore, a linear force-motion relation can be implied, and the frequency-domain approach can be applied to quickly estimate the short-term response statistics based on statistical assumptions. Here, the structural flexibilities are ignored, and the system transfer function is linearised.

For a floating platform, the body-fixed, right-handed cartesian coordinate system is illustrated in Figure 3. The system origin is at the still water level, with the positive z-direction pointing upwards. The six degrees of freedom shown in the figure are of interest in this study.
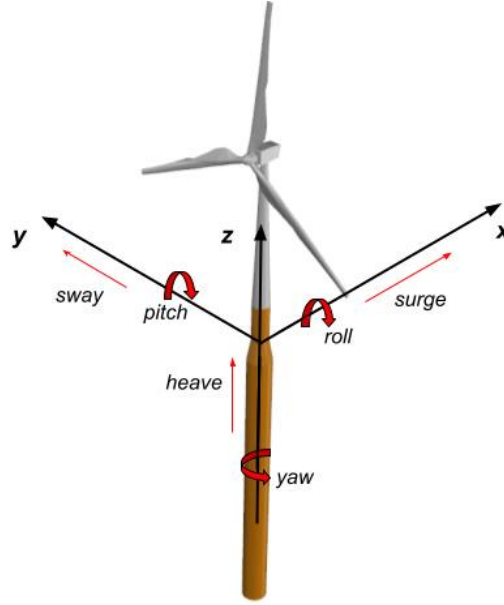
Figure 3. Body-fixed coordinate system for FOWT and degrees of freedom.

For a floating body with 6 DOFs, the equation of motion can be presented as follows

$$(M + A) \cdot \ddot{x} + B \cdot \dot{x} + C \cdot x = F \tag{1}$$

where M is the system mass matrix, A and B are the frequency-dependent hydrodynamic added mass and damping matrices, C is the stiffness matrix, and F is the excitation force. Here, the linear damping matrix consists of the hydrodynamic radiation damping and the linearised viscous damping, and the stiffness matrix includes the hydrostatic stiffness and the linearised mooring stiffness.

The solution to Equation (1) is the response amplitude operators (RAOs). To obtain the RAOs of an FOWT, the mass matrices of the systems are obtained by creating finite element models of the whole FOWTs with distributed mass in GeniE [15] followed by establishing the 6×6 mass matrix. The hydrodynamic analysis is carried out using a potential-flow solver WADAM [16]. The effects of irregular frequencies are also removed to exclude the spikes of body response caused at the frequencies where artificial sloshing resonance modes inside the body take place [17]. When solving for the RAOs, additional restoring matrices corresponding to the linearised stiffness of the mooring lines are specified such that the mooring effects are considered. The models are simulated as a set of regular waves within a frequency range from 0 to 0.5 Hz for different headings with an interval of 10 degrees to obtain the RAOs of the floaters as a function of excitation frequency for each heading.

2.2. Short-term statistics

Short-term statistics is applied in this study to estimate the response statistics of the floaters in a sea state for a given reference time. The basic assumption is that each short-term sea state is stationary, and the platform motion responses are Gaussian. Based on the RAOs, statistical values of the responses can be calculated, including the short-term extremes or response standard deviation of the displacement, velocity, and acceleration for a specified point on an

FOWT. The 3 hours reference time is chosen for the short-term statistics calculation as recommended for simulations of irregular sea states [18], [19].

Two different wave spectra are considered to model the sea conditions to observe the sensitivity of the floaters' response with respect to the wave spectral models:
- The JONSWAP which is a modified/peak-enhanced Pierson-Moskowitz spectrum.
- The Torsethaugen wave spectrum which is a 2-peaked spectral model developed for the Northern sea.

Each load case is considered a fully developed sea and is modelled separately by the JONSWAP and Torsethaugen spectra. The recommended nondimensional peak shape parameter (γ) and spectral width parameters (σ_a, σ_b), which are derived from experimental data, are used to form the spectral models [17]. The spectral density is calculated for each loading condition as a function of wave frequency.

The RAOs in this study are calculated for the nacelle level (1.7 m, 0 m, 89.6 m) and the platform level (0 m, 0 m, 10.0 m) since these are the locations where maintenance personnel spend the most time during their work. The response spectra for the floaters, $R_{ij}(\omega, \beta)$, are calculated for each degree of freedom as a function of wave frequency, ω, and wave heading, β, for each load case as

$$R_{ij}(\omega, \beta) = |\eta_i(\omega, \beta)|^2 \, S_j(\omega), \tag{2}$$

where the index i represents the degree of freedom (surge=1, sway=2, heave=3, roll=4, pitch=5, yaw=6), $\eta_i(\omega, \beta)$ represents the RAO of the relevant mode of the motion in each DOF, $S_j(\omega, \beta)$ represents the spectral density as a function of wave frequency for load case j. RMS values of the motions for each DOF and sea state are further derived from the relevant response spectrum. RMS motions are derived from the square root of the zero[th] moment of the response spectrum, $m_{i,j}$.

$$m_{i,j} = \int_0^{2\pi} \int_0^\infty \omega^0 \, R_{ij}(\omega, \beta) d\omega d\beta \tag{3}$$

$$rms_{ij} = \sqrt{m_{i,j}} \tag{4}$$

2.3. Metocean data

During the maintenance of the FOWTs the rotor blades are set to a parked position. Therefore, the wind loads are assumed negligible and are not included in this study. Overall significant wave height, spectral peak period, and wave heading are used to model the sea state in each load case in the later simulation study for two selected locations in Norway and South Korea.

A reduced dataset of ~500 load cases have been selected with a good representation of the distributions for significant wave height, spectral peak period, and wave heading, from hindcast data for two locations relevant for deployment of floating wind turbines at the coast of Norway and South Korea. The load cases have been selected from 100 000 random draws of ~500 load cases from the hindcast database, where the random draw with best correlation with the distributions was selected.

Hindcast data for the South Korean location include 25 years of data that are reduced to 502 load cases, while the hindcast data for the Norwegian location include 40 years of data that are

reduced to 501 load cases. The correspondence between the distributions from the the hindcast data set and the reduced data set used in this study are shown for both locations in Figure 4. The good corrspondence observed for both locations indicate that the reduced set of load cases should be representative when considering environmental conditions during maintenance operations.

A comparison of the distributions of the significant wave heights and spectral peak periods for the reduced set of load cases used in the analyses for Norway and South Korea are shown in Figure 5. Harsher wave conditions are observed for the Norwegian location with higher significant wave heights and higher spectral peak periods compared to the South Korean location.
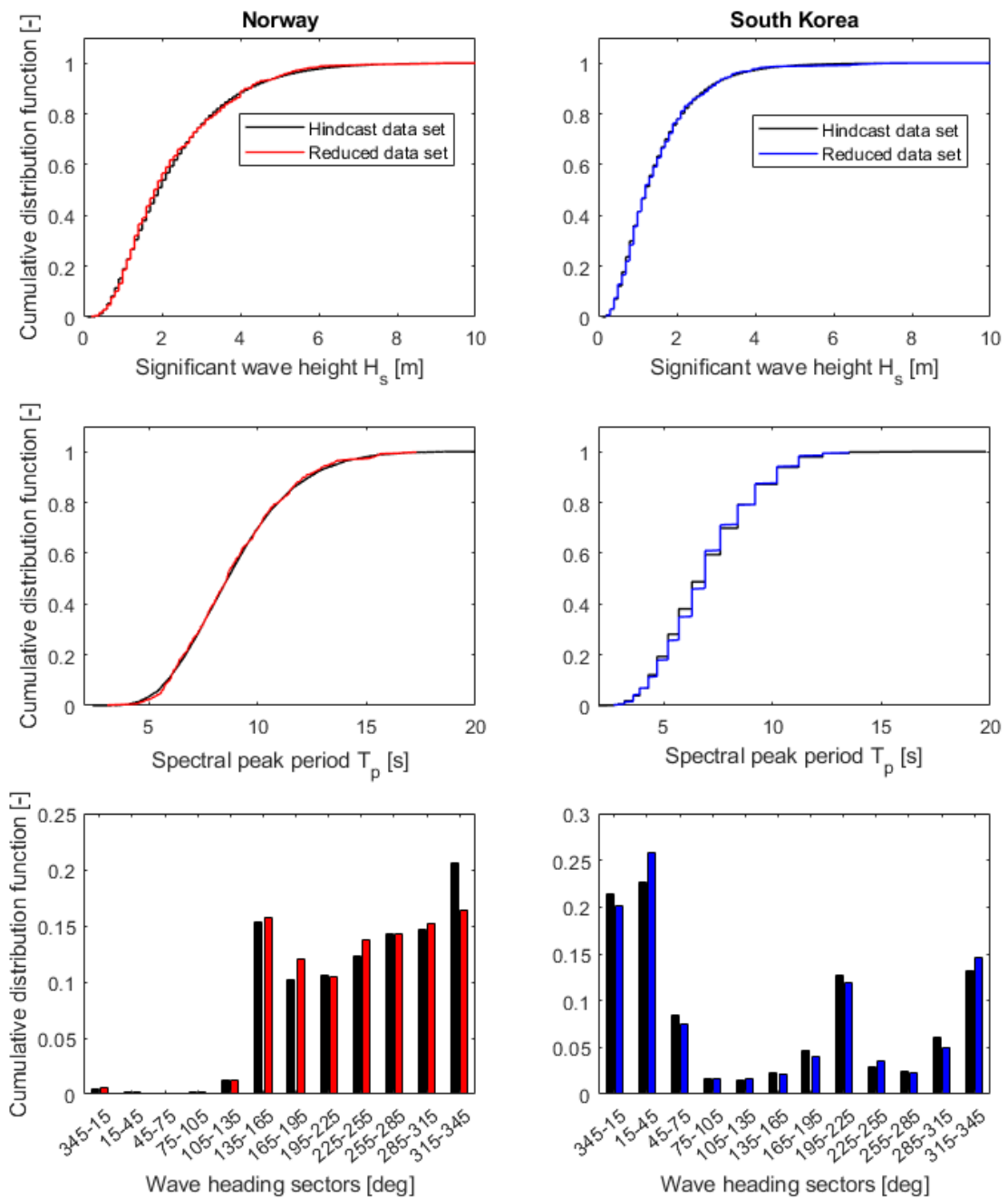
Figure 4. Comparison of the cumulative distributions of significant wave height (top), the cumulative distribution of spectral peak period (middle), and the distribution of wave heading sectors (bottom). Distributions for Norway (left) with hindcast data set (black) and reduced data set (red). Distributions for South Korea (right) with hindcast data set (black) and reduced data set (blue).
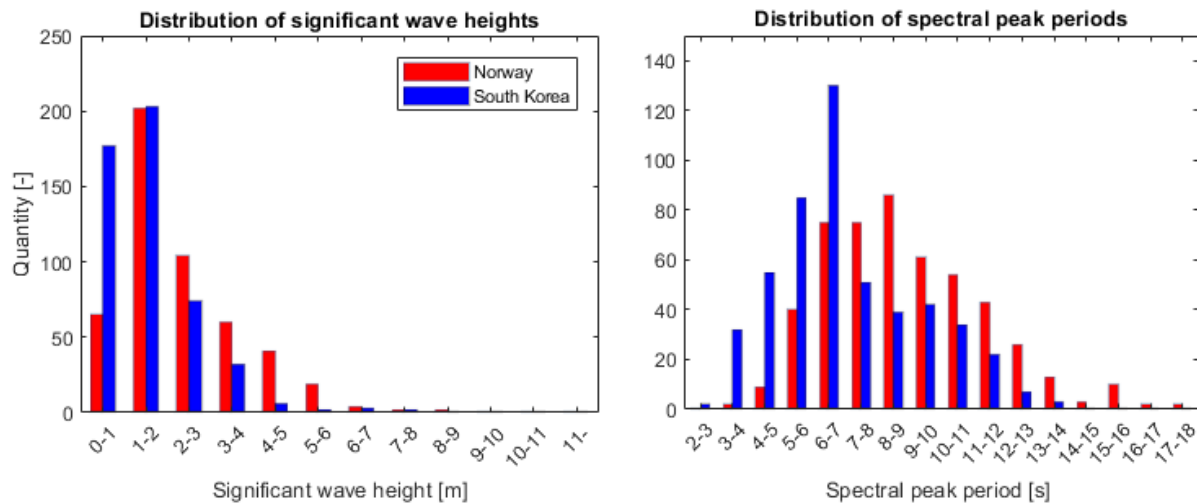
Figure 5. Distributions of significant wave heights (left) and spectral peak periods (right) from the reduced set of load cases for Norway (red) and South Korea (blue).

2.4. Derivation of limiting sea states

Motion signals that are derived from short-term statistics are evaluated against a set of limiting criteria based on a publication by the Nordic Research Collaboration [11] which is referenced and used in assessment criteria by several researches [8], [20], [21] regarding exposure of humans to vibration. The threshold levels for rotations, vertical and lateral accelerations are given as root mean square values. The limiting criteria from [11] based on the type of work that is going to be performed are presented in Table 1.

Table 1. Set of criteria with regards to vertical/lateral accelerations and rotational displacement **[11]**.

Description	Vertical acceleration (RMS)	Lateral acceleration (RMS)	Rotational displacement (RMS)
Light manual work*	0.20g	0.10g	6.0°
Heavy manual work	0.15g	0.07g	4.0°
Intellectual work**	0.10g	0.05g	3.0°
Transit passenger***	0.05g	0.04g	2.5°
Cruise liner	0.02g	0.03g	2.0°

* *Tolerable less than 1 hour* **[22]**
**   *0.5 hour exposure for people unused to ship motions* **[23]**.
***   *2 hour exposure for people unused to ship motions* **[23]**.

The maintenance work in the FOWTs, which typically takes 12 hours as a combination of 10 hours spent on the floater and 2 hours spent on the transit vessel, is often demanding and could require accuracy and high concentration of the personnel [8]. The "Intellectual Work'' criterion

represents reference values for "half an hour exposure period for people unused to ship motions'' while "Transit Passenger'' stands for a set of reference values for people in the same category but two hours exposure [23]. Only two hours do not reflect the real exposure time of the maintenance personnel during their work onboard an FOWT. Hence the ''Transit Passenger'' criterion is found the most relevant, since it is the longest time frame reference value for "people who are not used to be exposed to vessel motions". Therefore, "Transit Passenger" is chosen as the limiting criterion in this study, in line with [8].

2.5. Definition of workability index

The concept of a Workability Index (WI) presented by [8] is also utilised in this study to present the performances of different floaters with respect to exposure of maintenance personnel to motion. RMS values for rotational motion, lateral and vertical accelerations are calculated for each load case and are assessed against the limiting criteria. Load cases with any mode of the RMS motion responses exceeding the corresponding threshold are considered unworkable.

Subsets of load cases are defined below selected threshold levels for the significant wave height, and the WI within a subset can be defined as

$$WI = \frac{\sum_{j=1}^{m} q_j}{\sum_{i=1}^{n} q_i},\qquad(5)$$

where q_j represents the probability of a workable load case in the subset, m is the number of workable load cases, q_i represents the probability of a load case in the subset, and n is the number of load cases within the subset. The WI within a subset ranges between 0 and 1, where WI=1 corresponds to 100% workability within a the subset.

3. Spar and semi-submersible floating wind concepts

A spar and two different semisubmersible floaters are selected in this study since spars and semisubmersibles are currently the dominating floating offshore wind turbine concepts. The following three well-defined reference models that are all designed to support the NREL 5-MW reference wind turbine [24] are considered in this study:

- The OC3-Hywind [25] which was developed for the Offshore Code Comparison Collaboration (OC3) as part of Phase IV.
- The CSC-Semisubmersible [26] that was developed as a reference semi-submersible wind turbine within the Norwegian Research Centre for Offshore Wind Technology (NOWITECH).
- The generic 5 MW WindFloat concept reported in [27].

All three concepts have been tested in model scale experiments [27], [28], [29], while the Hywind and WindFloat concepts have also been deployed in full scale in several projects.

3.1. OC3-Hywind, CSC-Semisubmersible and WindFloat

The main partulars the floating wind turbine concepts are shown in Table 2, with the corresponding the geometries shown in Figure 6. The most protuding differences between the concepts are that

- The OC-3 Hywind achieves its basic stability from ballasting with its center of gravity (COG) far below the center of buoyancy (COB). Both the CSC-Semisubmersible and WindFloat achieve their basic stability from their well distributed waterplane area. However, it is noted that the vertical distance between the COG and COB are quite different between the two semisubmersibles. The vertical location of the COB is 3.6 m above the COG for CSC-Semisubmersible, while the corresponding distance is 12.3 mfor WindFloat.
- The CSC-Semisubmersible has the largest mass, which is 29% larger than OC3-Hywind and 122.8% larger than Windfloat.
- The draft of OC3-Hywind is naturally by far the deepest, but the difference between the two semisubmersible concepts is also significant, with the CSC-Semisubmersible having a 76.5% deeper draft than WindFloat. The deep draft of the CSC-Semisubmersible could make installation from a conventional quay challenging, and thereby losing an important advantage of the semisubmersible type FOWTs.
- The CSC-Semisumersible is a braceless structure with 4 columns where the wind turbine is placed on a center-column, while WindFloat is a semisubmersible with braces with 3 columns where the wind turbine is placed on one of the columns.

Despite the above differences it is seen that the differences in natural period is not that large. All three concepts have natural periods in heave and pitch that are above the typical range of wave periods with heave natural periods ranging between 19.9 s – 31.3 s and pitch natural periods ranging between 29.4s – 43.2 s.

Table 2. Main particulars of reference models.

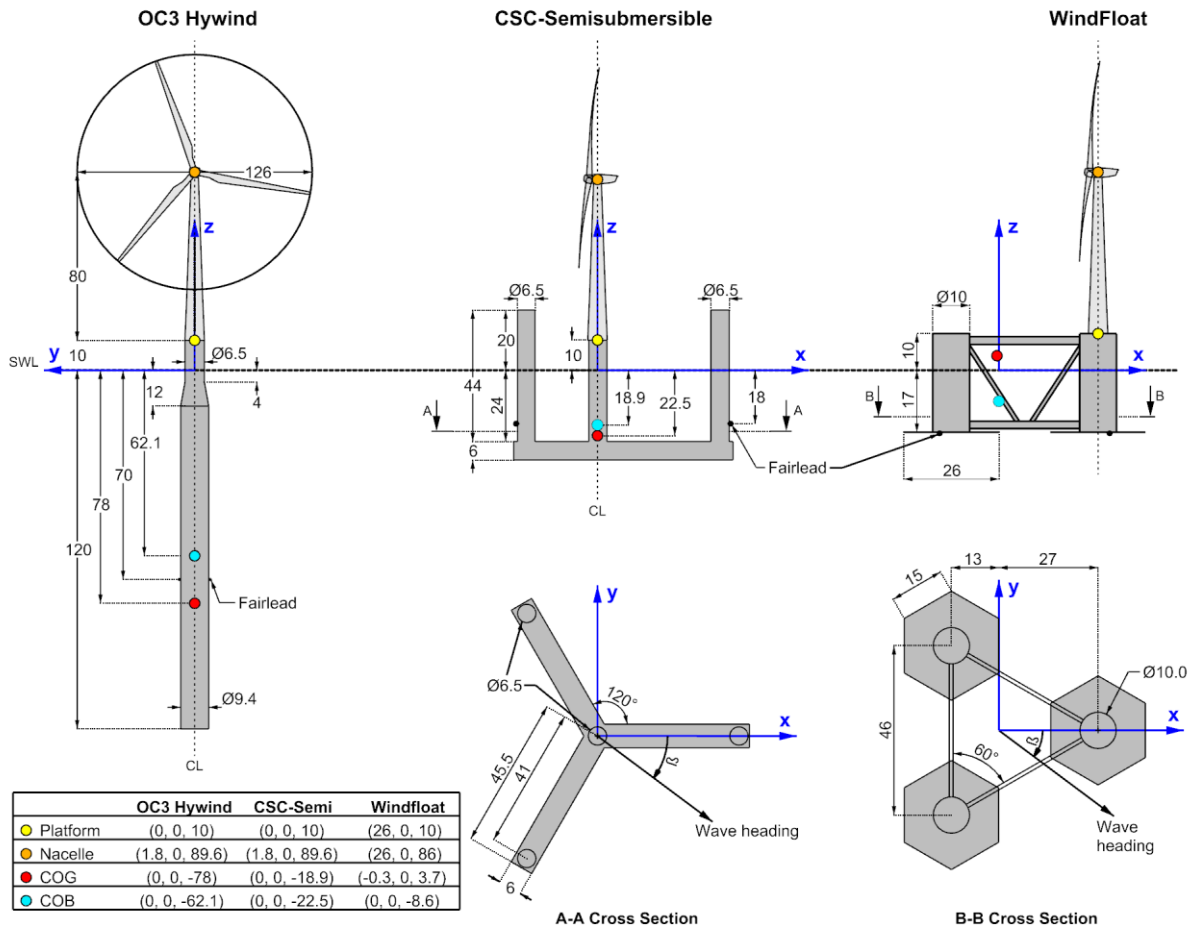| Parameter	OC3-Hywind	CSC-Semisubmersible	WindFloat
Mass	8014 t	10337 t	4640 t
Displacement	8177 t	10503 t	4640 t
Pre-tension at fairlead	163 t	166 t	54.5 t
Location of COG	(0, 0, -78) m	(0,0, -18.9) m	(-0.278, 0.0, 3.728) m
Location of COB	(0, 0, -62.1) m	(0, 0, -22.5) m	(-1.7, 0.0, 2.8) m
Draft	120 m	30 m	17 m
Surge natural period	125.0 s	76.9 s	108.6 s
Heave natural period	31.3 s	25.6 s	19.9 s
Pitch natural period	29.4 s	31.3 s	43.2 s

Figure 6. Geometry of reference models; OC3-Hywind (left), CSC-Semisubmersible (middle) and WindFloat (right). Dimensions are given in meters.

OC3-Hywind is a slender and cylindrical shaped structure with a deep draft of 120 m. The bottom part of the cylinder is filled with water and fixed ballast to create a positive righting lever when the structure is tilted, by keeping its centre of gravity (COG) lower than the centre of buoyancy (COB). The diameter of the structure is 9.4 m from the keel until 12 m beneath the free surface. The cylinder's diameter is tapered down from 9.4 m to 6.5 m starting from that level. The reduced diameter in the wave zone will reduce the wave loads and the reduced area in the water plane will increase the natural period in heave.

The CSC-Semisubmersible is a braceless hull with a symmetrical shape, but with a more complicated geometry compared to the OC3-Hywind. It consists of one central column and 3 outer columns mounted on 3 pontoons that are aligned with 120° in between. Each column has a diameter of 6.5 m and height of 44 m while the central column is 10 m shorter than the rest. The CSC-Semisubmersible is mainly stabilised by its well-distributed waterplane area and submerged volume that allows COB to shift to the more submerged side and create a positive righting moment when displaced.

The WindFloat is an asymmetric semisubmersible floater with braces between three columns and the wind turbine tower is placed on top of one of the columns. Water entrapment plates are

placed on the bottom of the columns to increase the added mass in heave such that the natural period in heave is outside the typical range of wave periods, but also to provide additional damping. Further, an active ballast system transfer water between the columns to keep the platform upright against the wind direction.

All concepts have the connection of the tower structure and the floating platform 10 m above the SWL. The OC3 Hywind and the CSC-Semisubmersible have and a nacelle level at 89.6 m height, while WindFloat has a nacelle level of 86.0 m.

The mooring system for the OC3 Hywind and the CSC-Semisubmersible concepts is composed of three catenary chain mooring lines. WindFloat use a catenary mooring system with 4 mooring lines, where two of the mooring lines are placed on the column with the wind turbine. Each mooring line on WindFloat consist of segments with chain on the top and the bottom with polyester rope in between and includes a clump weight. For all concepts, one end of the mooring line is connected to the fairlead on the floater while the other end is connected to an anchor that is buried under the soil on the seabed.

3.2. Model Validations

3D panel models are created for the different FOWT concepts. The OC3-Hywind panel model consists of approximately 4000 rectangular panels while CSC-Semisubmersible's model is formed with approximately 2000 panels. The WindFloat panel model has approximately 9000 panels due to complexity of the geometry. The largest panel and mesh size are set to 1x1 m^2 and 0.25x0.25 m^2 respectively for all models.

To validate the accuracy of the hydrodynamic models developed for this study – denoted as the present models - a frequency domain response analysis is performed. These results are compared with corresponding results from the original publications of the OC3-Hywind [25], CSC-Semisubmersible [26], and WindFloat [27] – denoted as the reference models. The wind turbine is considered rigid in all models, and only regular waves are considered. Wind and current loads are neglected. Comparison of the RAOs from the present models and reference models are shown for OC3-Hywind, CSC-Semisubmersible and WindFloat in Figure 7 - Figure 9.

Generally good agreement is observed between the reference and present models for all concepts and motions considered.
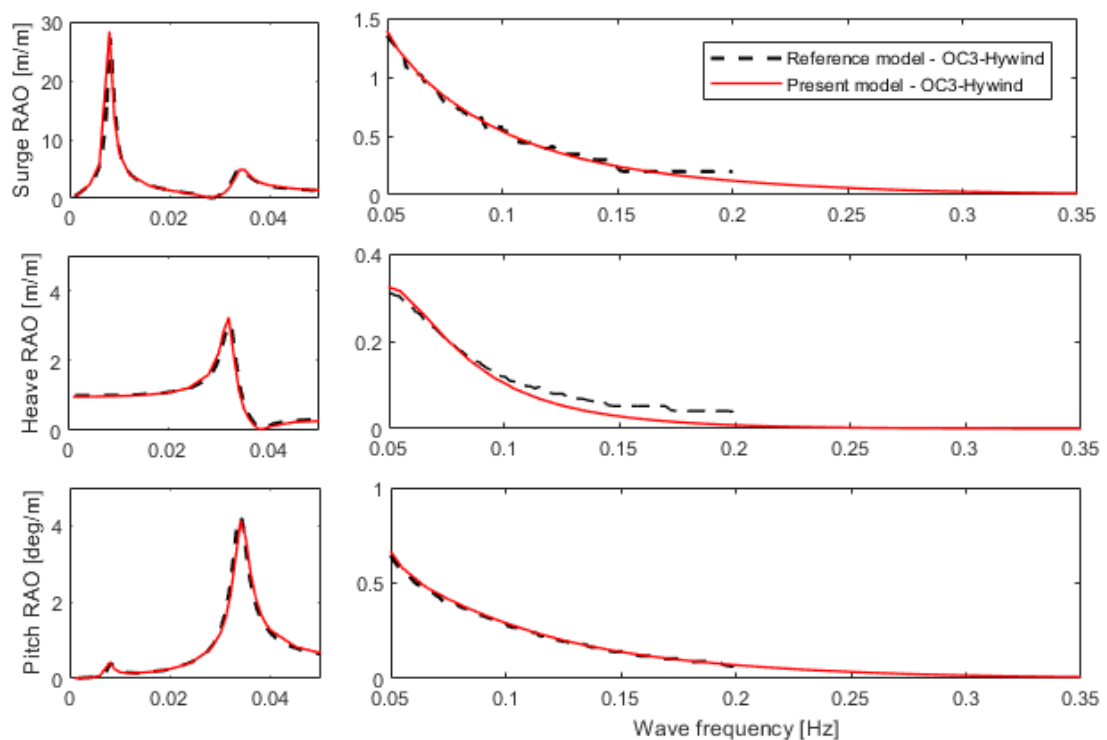

Figure 19. Surge (top), heave (middle), and pitch (bottom) RAO's for the reference OC3-Hywind model from [25] (dashed black) and the present OC3-Hywind model (red), that is used in this study when excited by regular waves with 0° wave heading.
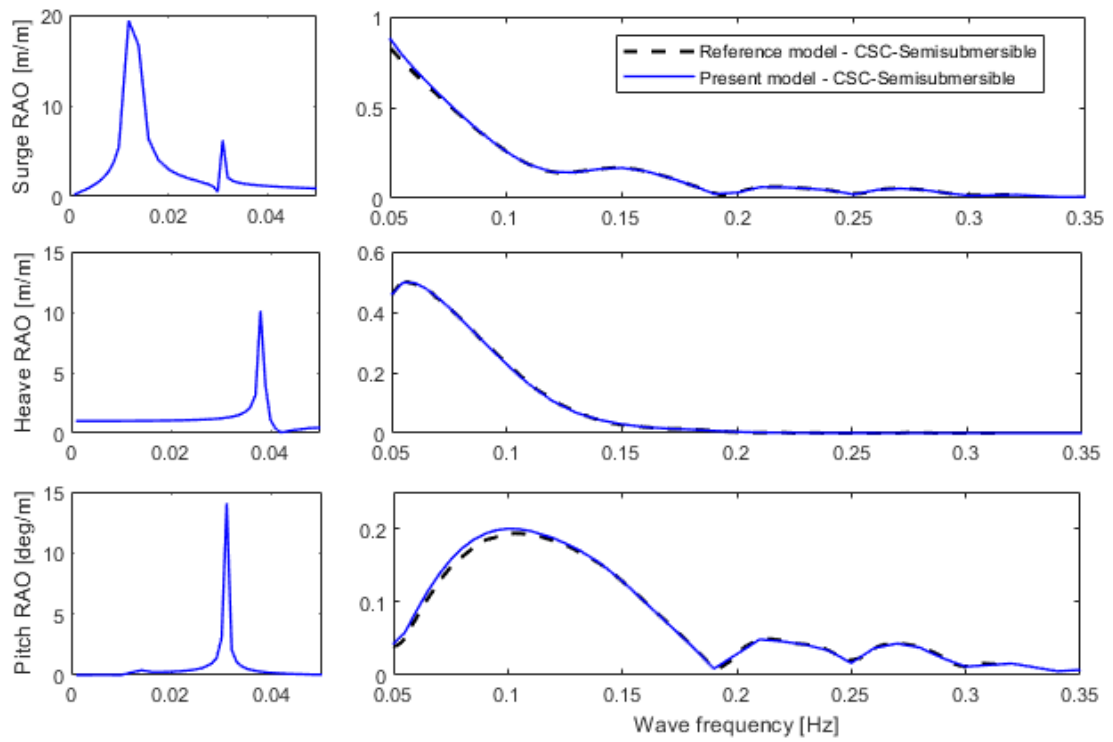
 Figure 20. Surge (top), heave (middle), and pitch (bottom) RAO's for the reference CSC-Semisubmersible model from [26] (black) and the present CSC-Semisubmersible model that is used in this study (red), when excited by regular waves with 0° wave heading.
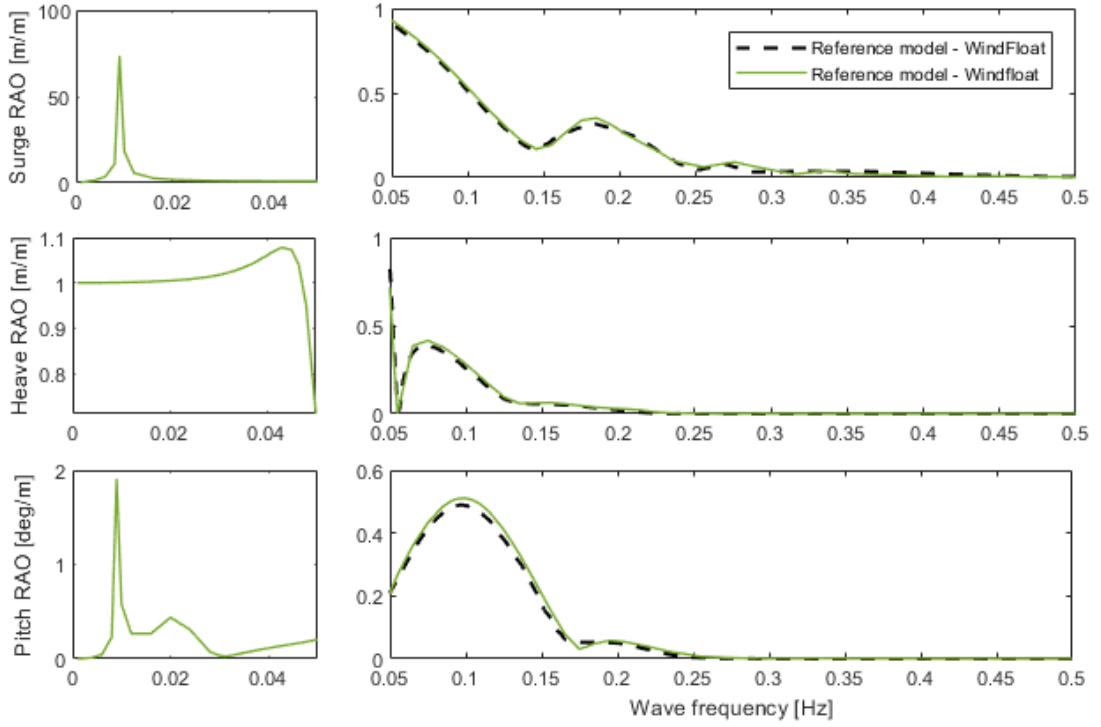
Figure 9. Surge (top), heave (middle), and pitch (bottom) RAO's for the reference WindFloat model from **[27]** (dashed black) and the present WindFloat model that is used in this study (green), when excited by regular waves with 0° wave heading.

4. Dynamic properties

4.1. Center of rotation

The vertical center of rotation of a floating structure can be considered as the frequency dependent vertical position without horizontal motion. The center of rotation is a useful dynamic property to understand the horizontal motions and accelerations at different vertical locations for different floater designs. Under the assumption of harmonic floater motions in surge, η_1 , heave, η_3 , and pitch, η_5, and generally small pitch angles, the horizontal surge motion at a given vertical position z is given as

$$\eta_{surge}(z) = \eta_1 + z\eta_5, \tag{6}$$

where $\eta_{surge}(z)$ is the surge motion at a vertical position z along the structure. From Equation (6) it is seen that $\eta_{surge}(z) = 0$ is achieved for

$$z = -\frac{\eta_1}{\eta_5} \tag{7}$$

Generally, the complex transfer function $H_i(\omega_j, \beta)$ between wave and motion response i is found as

$$H_i(\omega_j, \beta) = \frac{\eta_i(\omega_j, \beta)}{\zeta_{A_j}}, \qquad (8)$$

for a regular wave with frequency ω_j, amplitude ζ_{A_j} and wave heading β. Insertion of Equation (8) into Equation (7) gives the center of rotation on the form

$$z = \text{Re}\left\{ -\frac{|H_1(\omega_j)|}{|H_5(\omega_j)|} e^{i(\delta_{1j} - \delta_{5j})} \right\}, \qquad (7)$$

where δ_{ij} is the phase angle for motion response i at frequency j.

The frequency dependent center of rotation and the phase angle between surge and pitch motion are shown as function of wave frequency in Figure 10 for the OC3-Hywind, CSC Semisubmersible and WindFloat. It is seen that the center of rotation for OC3-Hywind does not change significantly with wave frequency, and that the surge and pitch motion of the OC3-Hywind are in phase for all wave frequencies. This is opposite to both the CSC-Semisubmersible and WindFloat. An advantageous property of both semisubmersible concepts, and WindFloat in particular, is that the center of rotation is close to the nacelle level at ~90 meter for wave frequencies around ~0.1 Hz where the wave energy content is typically high. This gives reduced structural fatigue damage due to wave induced motions at the nacelle in this frequency range. On the other hand, for wave frequencies around ~0.2 Hz, the center of rotation of both the CSC Semisubmersible and WindFloat are further from the nacelle than for OC3 Hywind. The center of rotation for WindFloat is above the nacelle level for higher wave frequencies, indicating that the horizontal motion at the platform level is larger than the horizontal motion at the nacelle level in this frequency range.
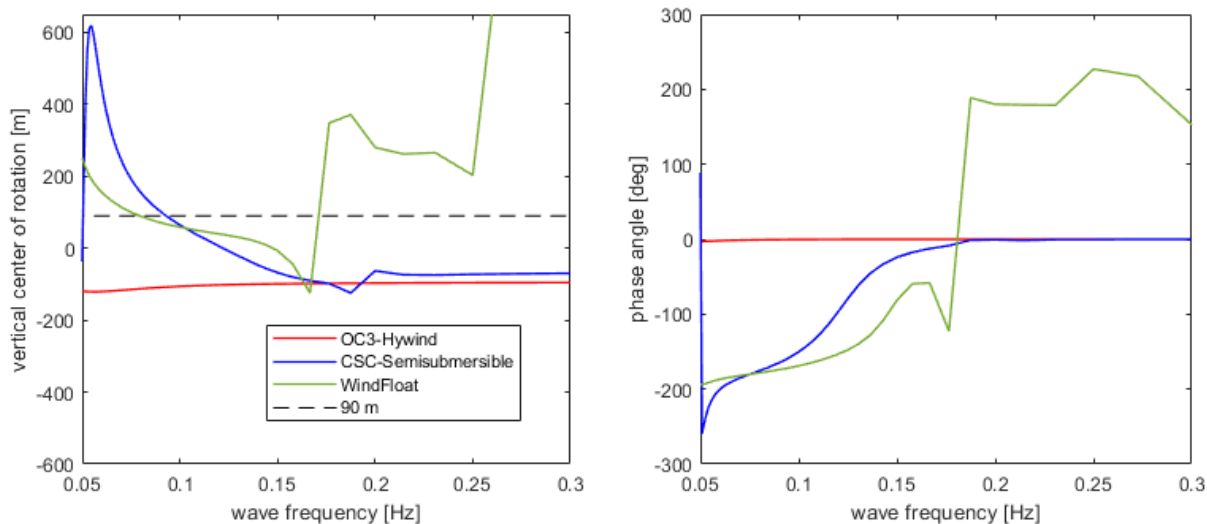
Figure 10. Vertical position of center of rotation (left) and phase angle between surge and pitch motion (right) for OC3 Hywind (red), CSC-Semisubmersible (blue), and WindFloat (green). The median nacelle level for the three floaters at 90 m is indicated (dashed black).

4.2. Wavelength and geometric properties of the CSC Semisubmersible and WindFloat

The geometry of buoyancy stabilised floaters in the wave zone can cause special peaks in the response spectrum depending on wavelength and wave heading. When the horizontal wave loads on the columns are in phase, the wavelength and heading are considered in the following.

By assuming infinite water depth, the wave period, T, corresponding to a given wavelength, λ, becomes [30]:

$$T = \sqrt{\frac{2\pi\lambda}{g}},$$ (8)

where g is the acceleration of gravity.

The wave loads on the columns of the CSC-Semisubmersible shown in in Figure 6 are in phase for the combinations of wave headings and wave periods shown in Table 3. Only wavelengths corresponding to wave periods larger than 3.0 s are considered. It is seen that the horizontal wave loads on the columns are in phase for a broad range of wave headings and wave periods.

Similarly, the wave loads on the columns of WindFloat shown in Figure 6 are in phase for the combinations of wave headings and wave periods shown in

.

Table 3. Combinations of wave directions and wave lengths and corresponding wave periods/frequencies – that are expected to give increased surge loading on the CSC-Semisubmersible due to the floater geometry in the wave zone.

Wave headings [deg]	Wave length [m]	Period [s]	Frequency [Hz]	Description
0, 60, 120, 180, 240, 300	20.5	3.62	0.276	Horizontal wave loads on all 4 columns in phase
0, 60, 120, 180, 240, 300	61.5	6.28	0.159	Horizontal wave loads on 3 outer columns in phase - center column 120 deg out of phase
0, 60, 120, 180, 240, 300	30.75	4.43	0.225	Horizontal wave loads on 3 outer columns in phase - center column 240 deg out of phase
30, 90, 150, 210, 270, 330	35.5	4.76	0.210	Horizontal wave loads on all 4 columns in phase
30, 90, 150, 210, 270, 330	17.75	3.37	0.300	Horizontal wave loads on all 4 columns in phase

Table 4. Combinations of wave directions and wave lengths and corresponding wave periods/frequencies – that are expected to give increased surge loading on WindFloat due to the floater geometry in the wave zone.

Wave headings [deg]	Wavelength [m]	Period [s]	Frequency [Hz]	Description
0, 60, 120, 180, 240, 300	39.8	5.05	0.198	Horizontal wave loads on all 3 columns in phase
0, 60, 120, 180, 240, 300	19.9	3.57	0.280	Horizontal wave loads on all 3 columns in phase
0, 60, 120, 180, 240, 300	13.3	2.91	0.343	Horizontal wave loads on all 3 columns in phase
30, 90, 150, 210, 270, 330	46	5.43	0.184	Horizontal wave loads on 2 columns in phase, one column 180 deg out of phase
30, 90, 150, 210, 270, 330	23	3.84	0.261	Horizontal wave loads on all 3 columns in phase

There is an extensive growth in the offshore wind industry both in terms of installed capacity and turbine size. Wind turbines with a rated generator capacity up to three times larger than the capacity of the NREL 5 MW wind turbine considered in this study could be deployed in some of the floating wind projects planned towards 2026 [5]. Hence, it is important to consider how the wave periods resulting in horizontal wave loads in phase on the columns change with an upscaling of the floater. The scaling of the floater model does not generally scale linearly with the wind turbine, and a variation in floater model scale from 1.0 to 2.0 is considered in the following. The floater models that are analysed in this study corresponds to a scale 1.0.

Figure 11 show how the wave periods leading to horizontal wave loads in phase on the different columns will change with different scaling for the CSC-Semisubmersible and WindFloat. It is seen that the wave periods will increase and that also even more periods will enter the wave period range when the scale is increased. When the wave periods increase from the lower end of the wave period range as shown in Figure 11, the associated horizontal wave loads are expected to increase. A larger significant wave height will typically be associated with a higher spectral peak period; and in addition the probability of occurrence of the sea state will typically increase. The latter is observed in the distributions in Figure 4 and Figure 5 for both the Norwegian and the South Korean locations considered in this study. In total, this indicates that the impact of horizontal wave loads in phase on the columns of semi-submersible FOWTs will increase with larger scale.
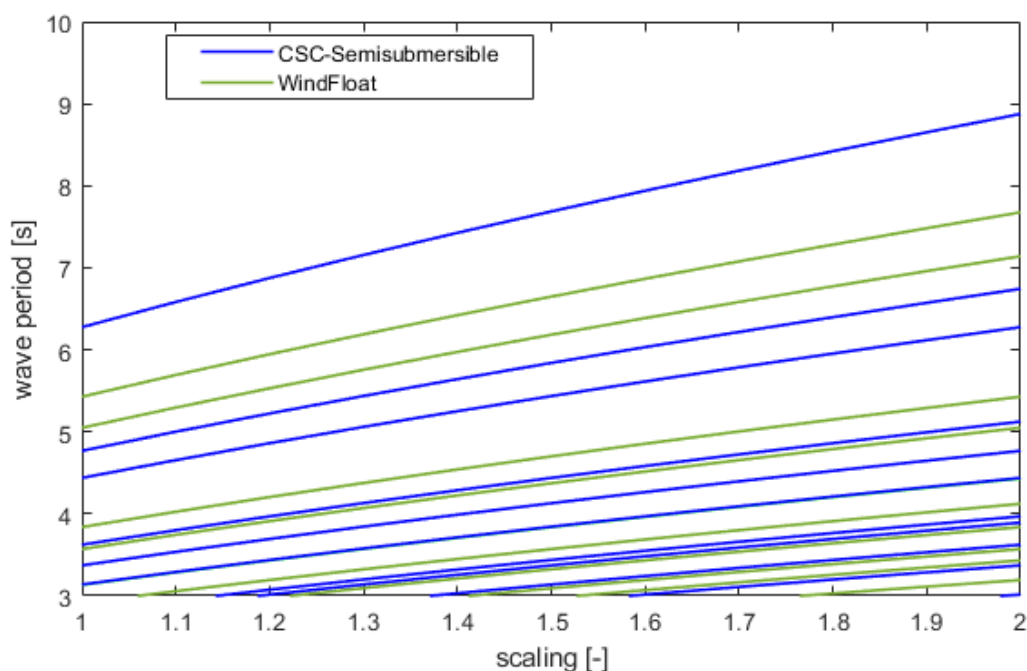

Figure 11. Effect of scaling on wave periods leading to horizontal wave loads in phase on the columns of CSC-Semisubmersible (blue) and WindFloat (green).

4.3. Comparison of RAOs relevant for human exposure

The pitch motion, as well as the lateral and vertical acceleration RAOs for the OC3-Hywind, CSC-Semisubmersible, and WindFloat are calculated along the dominant wave direction for several wave headings within the frequency range 0-0.5 Hz, respectively. The motions of the OC3-Hywind were found to be very little affected by the wave heading due to its symmetrical shape and negligible contribution from the catenary mooring system. For this reason, only results with $0°$ wave heading is presented for the OC3-Hywind.

 A comparison of the lateral and vertical accelerations at the platform and the nacelle level are shown in terms relative to the gravitational acceleration, g, in Figure 12 and Figure 13 respectively.A comparison of the pitch motion at SWL is shown in Figure 14. The following observations can be made from Figure 12– Figure 14:

- The lateral accelerations at the nacelle level are approximately a factor ~2 larger than the accelerations at the platform level for OC3-Hywind and CSC-Semisubmersible while the vertical accelerations are almost unaffected by the vertical level for both concepts.
- The largest acceleration peak at ~0.19 Hz is lower at the nacelle level than at the platform level for WindFloat. This can be explained by the location of the center of rotation above the nacelle level in this frequency range as shown in the left part of Figure 10. There is also has a shift in the peak frequency towards a lower frequency from the platform level to the nacelle level for WindFloat, The relative phase angle between surge and pitch in the right part of Figure 10 show that surge and pitch are approximately 180 degree out of phase at the peak frequency for the platform acceleration, while they are approximately in phase at the peak frequency of approximately 0.17 Hz for the nacelle acceleration, and could explain the shift in peak frequency between the platform and nacelle levels. The vertical accelerations of WindFloat are larger at the nacelle level than the platform level for other wave headings than 0 degrees, and the largest difference is observed for wave heading 60 degrees with 49 % increase in the peak acceleration RAO.
- The maximum peak values in the lateral nacelle acceleration RAOs within the wave frequency range (0.05 – 0.3 Hz) are quite similar among the three floater concepts, while the maximum peak value in the lateral platform acceleration RAOs are approximately a factor of 2 larger for WindFloat than for OC3-Hywind and CSC-Semisubmersible.
- The lateral accelerations of the CSC-Semisubmersible have significant variation with both wave heading and frequency. Different dominant peaks in the lateral accelerations are observed at certain wave headings at higher wave frequencies:
  - The acceleration responses for 0 and 60 degree wave heading are very similar due to symmetry of the CSC-Semisubmersible floater. It is seen that the three dominant peaks at higher wave frequencies for these wave headings correspond with the wave frequencies with horizontal wave loading in phase in Table 3.
  - The acceleration responses for 30 and 90 degree wave headings are also similar due to symmetry. The two dominant peaks at higher wave frequencies for these wave headings correspond with the wave frequencies with horizontal wave loading in phase in Table 3.

- The lateral accelerations of WindFloat have a similar variation with both wave heading and frequency as the CSC-Semisubmersible, and the dominant peaks in the platform lateral accelerations for WindFloat are in line with Table 4.
- The pitch motion RAOs show that the CSC-Semisubmersible has approximately half the pitch response of WindFloat in the wave frequency range, while OC3-Hywind is within the response range of the two semisubmersible concepts.
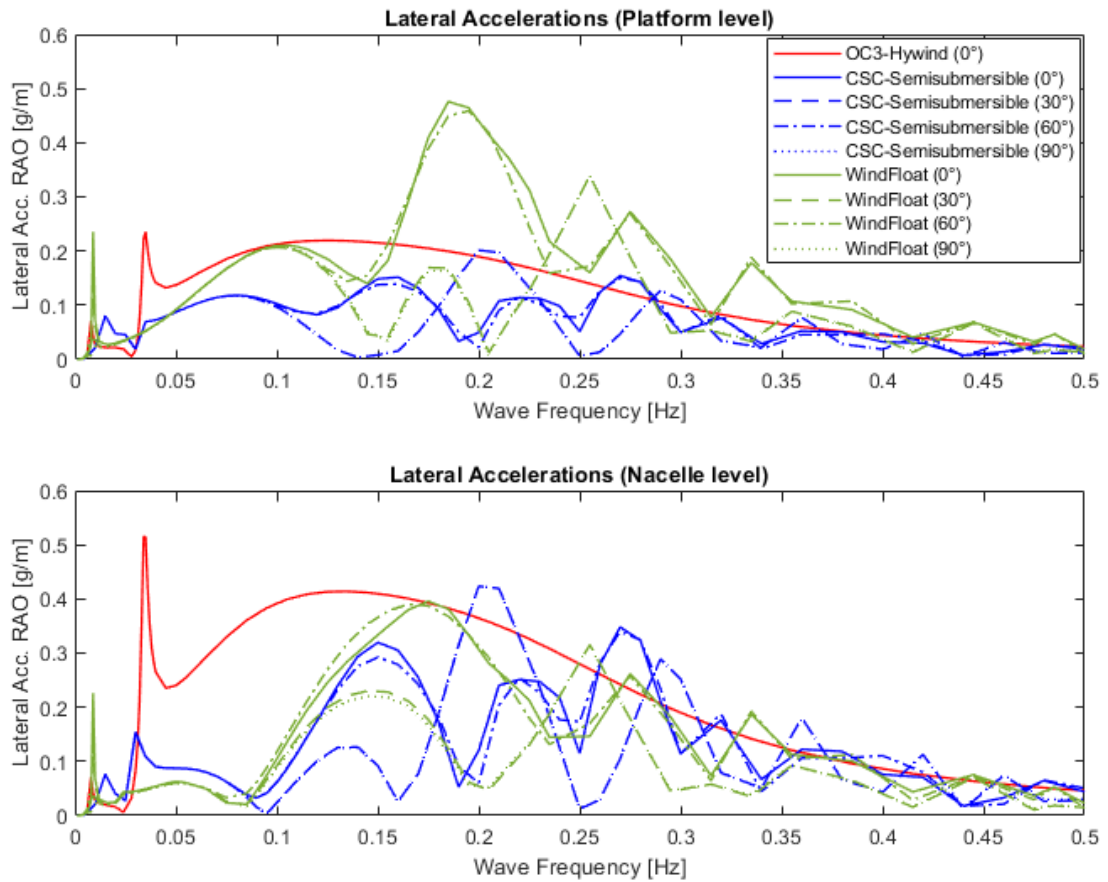

Figure 12. Lateral acceleration RAOs along the wave heading direction the OC3-Hywind (red), CSC-Semisubmersible (blue), and WindFloat (green) at the platform level (top) and at the nacelle level (bottom).
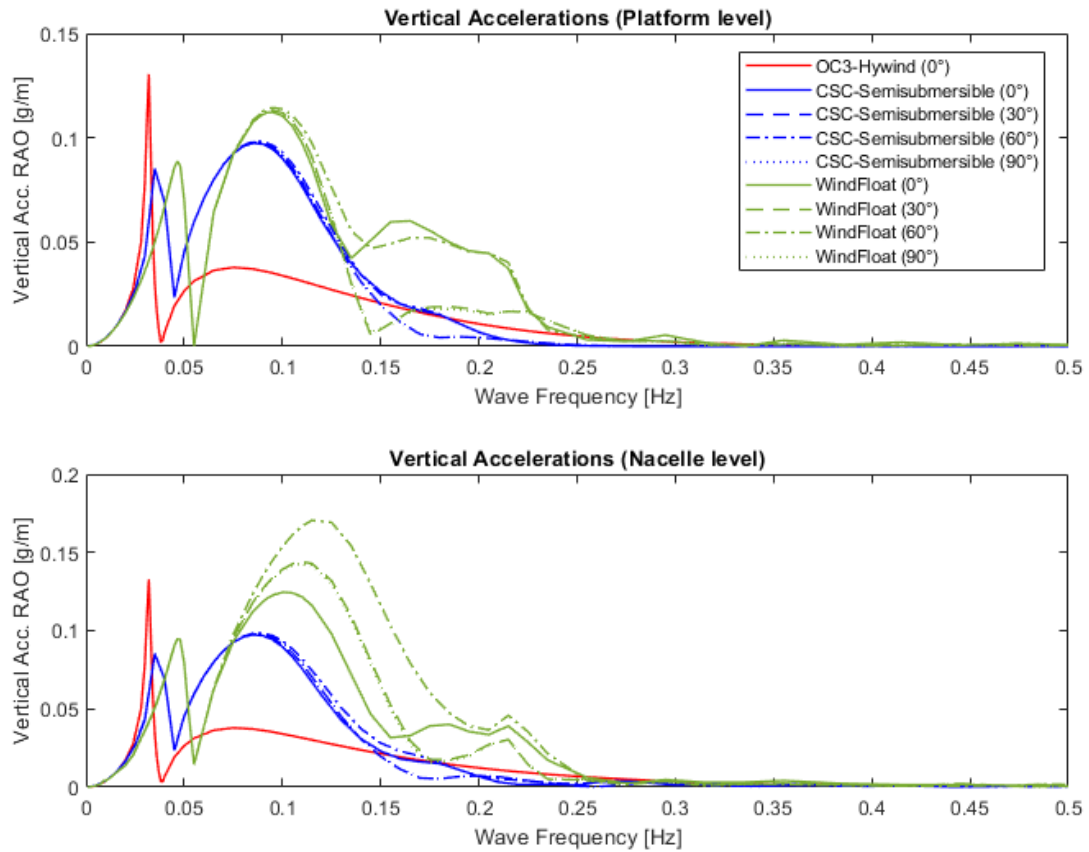
Figure 13. Vertical acceleration RAOs along the wave heading direction for the OC3-Hywind (red), CSC-Semisubmersible (blue), and WindFloat (green) at the platform level (top) and at the nacelle level (bottom).
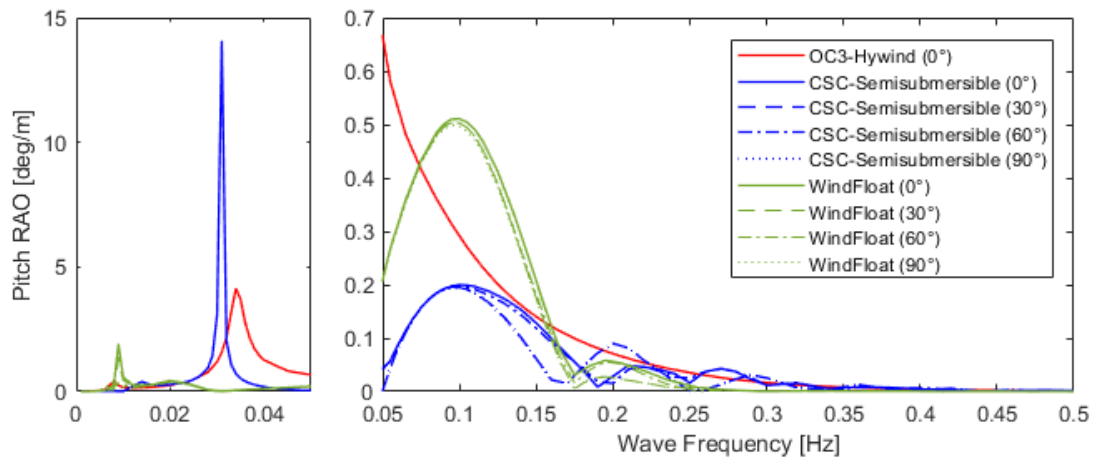

Figure 14. Pitch motion RAOs at SWL along the wave heading direction for the OC3-Hywind (red), CSC-Semisubmersible (blue), and WindFloat (green).]

5. Comparative simulation studies

5.1. Response contours from generic sea states

Generic RMS response contour plots for the relevant responses for motion sickness are developed by analysing the generic load case matrix with significant wave heights varying from 0-12 meter and spectral peak periods varying from 3 to 17 seconds for the three FOWT concepts. Each sea state is analysed using both the JONSWAP and Torsethaugen wave spectra.

The response contour plots for the RMS values for the lateral and vertical accelerations, and the rotational motion, are shown for OC3-Hywind, CSC-Semisubmersible, and WindFloat in Figure 15- Figure 18. It is evident that it is only the limiting RMS criterion related to lateral accelerations (0.04 g) that can potentially be exceeded for any of the concepts considered. The limiting RMS criteria for vertical acceleration (0.05 g) and angular motion (2.5 degrees) are not exceeded for any of the concepts, for any sea states, wave directions, or wave spectra considered. The focus in the following is therefore on the lateral accelerations.

Contour plots of the nacelle level lateral accelerations from analyses using the JONSWAP wave spectrum with 0 degree wave heading are shown in the upper part of Figure 15. The contour plots for OC3-Hywind have a flat curve as function of spectral peak period, while both semisubmersible concepts have clear peaks and troughs that can be related to the acceleration RAOs in Figure 12. Generally, OC3-Hywind has the highest nacelle acceleration level among the concepts, but WindFloat has a trough in the contour plot around 6 seconds to approximately the same level as OC3 Hywind. The CSC-Semisubmersible has the lowest nacelle acceleration level among the concepts.

The platform level lateral acceleration contour plots from analyses using the JONSWAP wave spectrum with 0 degree wave heading are shown in the upper part of Figure 16. OC3-Hywind and the CSC-Semisubmersible has improved contours for the platform level compared to the nacelle level. However, the contours for WindFloat are worse at the platform level than at the nacelle level, with a deep trough for spectral peak periods around 5 seconds at the platform level. These findings are in line with acceleration RAOs in Figure 12. It is also a clear indication that a person experiencing motion sickness should stay at the platform level onboard OC3-Hywind and CSC-Semisubmersible, and at the nacelle level onboard WindFloat.

Use of the double peaked Torsethaugen wave spectrum to generate the nacelle lateral acceleration contour plots for 0 degree wave heading are shown in the upper part of Figure 17. The lateral acceleration contours are found to be less curved compared to the corresponding contours using the JONSWAP wave spectrum in Figure 15:
  - The contours for OC3 Hywind has increased accelerations at low wave periods due to contribution from the low frequency peak in the double-peaked Torsethaugen wave spectrum. On the other hand, the accelerations at the trough spectral peak period is reduced due to the contribution from the high frequency peak in the Torsethaugen wave spectrum.
  - The lateral acceleration contours for both semisubmersible floaters are both reduced and less curved since the energy content at the relatively narrow troughs in spectral peak period range will be reduced when using a double peaked wave spectrum.

The effect of a wave heading of 30 degree on the nacelle lateral accelerations from analyses using the JONSWAP wave spectrum are shown for CSC-Semisubmersible and WindFloat in the upper part of the contour plots in Figure 18:

- The contours for the CSC-Semisubmersible have changed from having two troughs at 0 degrees wave heading to having one trough at 30 degrees wave heading. The acceleration level at the single trough is about the same level as at the largest trough for 0 degrees wave heading. The frequency of the trough is shifted to between the two troughs at 0 degree wave heading. This is in line with the nacelle lateral acceleration RAOs in Figure 12.
- The nacelle acceleration contours for WindFloat is significantly improved for 30 degree wave heading and WindFloat has smallest nacelle lateral accelerations among the concept for this wave heading. This is also in line with the nacelle lateral acceleration RAOs in Figure 12.
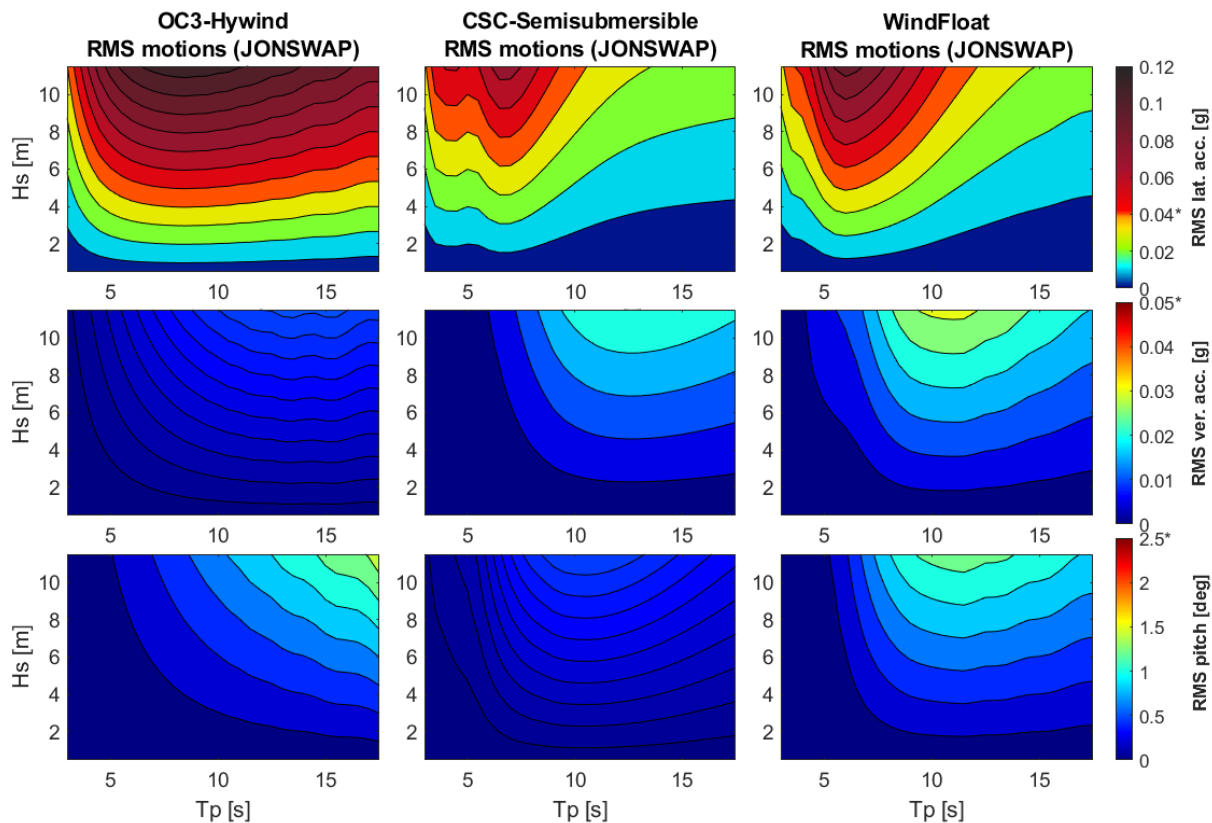

Figure 15. *Nacelle level* response contour plots for the OC3-Hywind (left), CSC-Semisubmersible (middle) and WindFloat (right) from generic load cases using the JONSWAP wave spectrum with 0° wave heading. RMS values of lateral accelerations (top), vertical accelerations (middle), and pitch motion (bottom) at the *nacelle* level. The limiting RMS value is indicated with an asterisk (*) in the contour color axes on the right hand side.
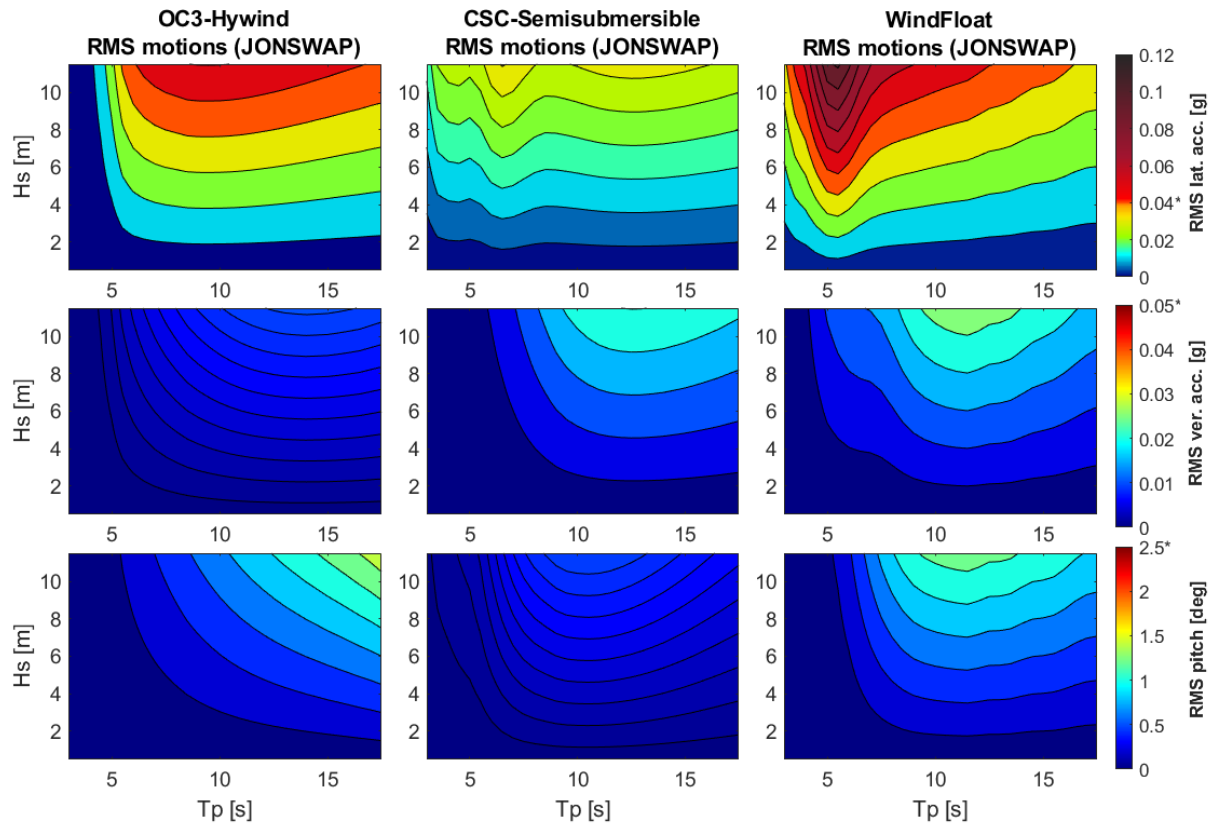
Figure 16. *Platform level* response contour plots for the OC3-Hywind (left), CSC-Semisubmersible (middle) and WindFloat (right) from generic load cases using the JONSWAP wave spectrum with 0° wave heading. RMS values of lateral accelerations (top), vertical accelerations (middle), and pitch motion (bottom). The limiting RMS value is indicated with an asterisk (*) in the contour color axes on the right hand side.
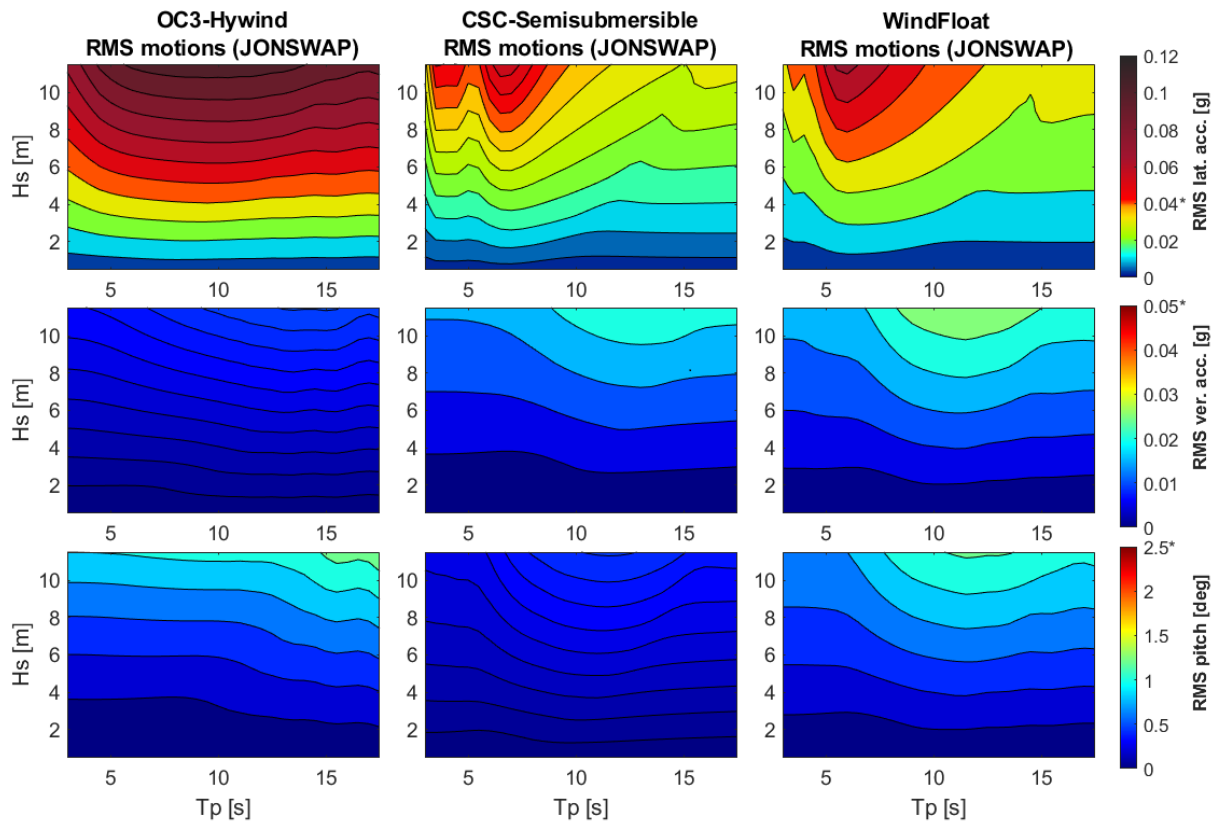
Figure 17. *Nacelle level* response contour plots for the OC3-Hywind (left), CSC-Semisubmersible (middle) and WindFloat (right) from generic load cases using the Torsethaugen wave spectrum with 0° wave heading. RMS values of lateral accelerations (top), vertical accelerations (middle), and pitch motion (bottom) at the *nacelle* level. The limiting RMS value is indicated with an asterisk (*) in the contour color axes on the right hand side.
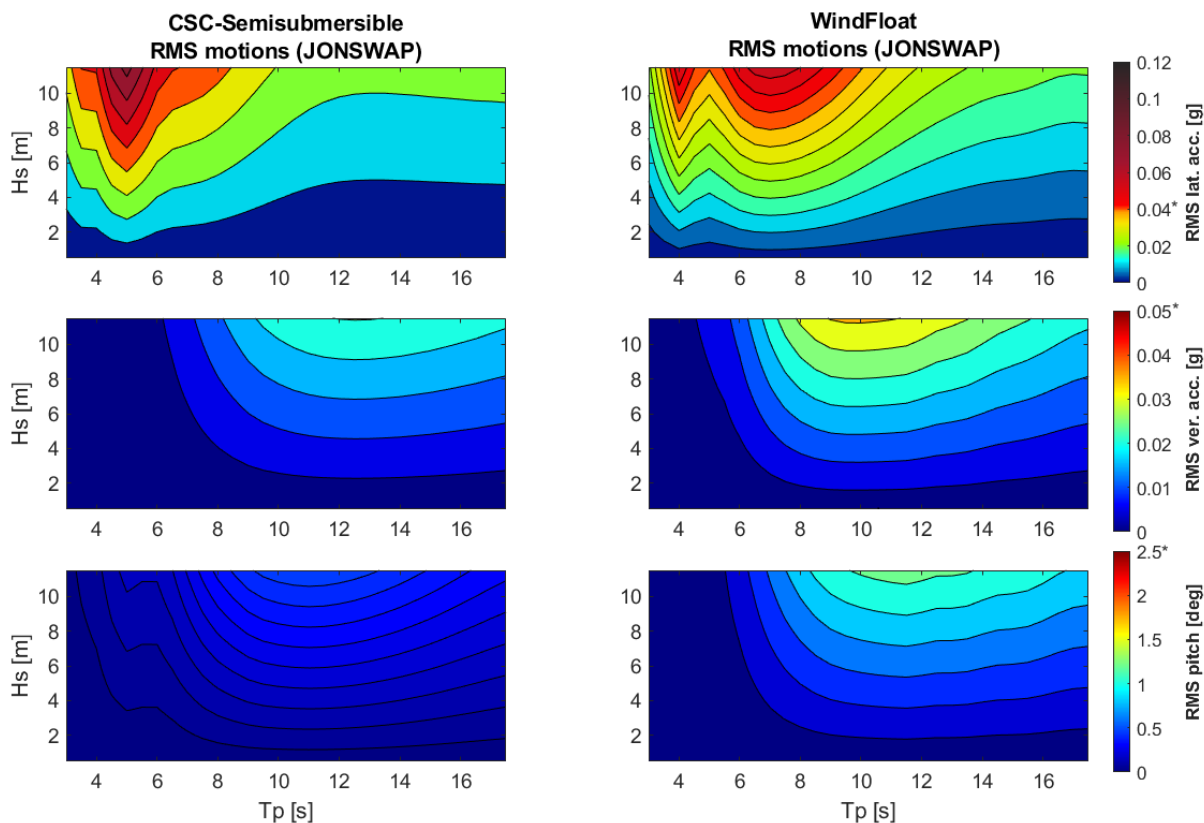
Figure 18. *Nacelle level* response contour plots for the CSC-Semisubmersible (left) and WindFloat (right) using the JONSWAP wave spectrum with 30° wave heading. RMS values of lateral accelerations (top), vertical accelerations (middle), and pitch motion (bottom). The limiting RMS value is indicated with an asterisk (*) in the contour color axes on the right hand side.

5.2. Calculation of workability index for two specific locations

The workability index from Equation (5) is calculated for several threshold levels for the significant wave height for OC3-Hywind, CSC-Semisubmersible, and WindFloat for two locations relevant for floating wind deployment. One location is at the coast of Norway and the other location is at the coast of South Korea, and the reduced metocean data sets from Figure 4 are applied in the analyses.

The operational limit related to the significant wave height is strongly dependent on the type of vessel used for crew transfers. CTVs vary from 1.5-2.5 m in operational limit, while conventional SOVs with 8-10 times higher daily rate can operate in harsher sea conditions with significant wave height up to 4.5-5.0 meter [6].

The workability index of the three FOWT concepts are shown as function of limiting significant wave height for both locations in Figure 19 and Figure 20. The workability index for work on the platform level is shown in Figure 19. The workability index for the platform level is 1 for significant wave heights up to 5 m regardless of concept, location, and wave spectrum used in the analyses.

The workability index for work on the nacelle level is shown in Figure 20. The workability index for the nacelle level is 1 for significant wave heights up to 3.5 m regardless of concept, location, and wave spectrum used in the analyses. The significant wave height of 3.5 m

corresponds to the maximum significant wave height for crew transfers to FOWTs reported in [8]. Both semisubmersible concepts have a workability index of 1 even for significant wave heights up to 5 m. OC3-Hywind has a reduction in workability index for significant wave heights above 3.5 m due to exceedance of the limiting RMS criteria on lateral accelerations (0.04 g):

- The reduction in workability index is largest when using the JONSWAP wave spectrum at both locations, which is in correspondence with the lateral acceleration contour plots in Figure 15 and Figure 17.
- The reduction in workability index is significantly larger at the Norwegian location compared to the South Korean location. This is probably due to the higher probability of low spectral peak periods at the South Korean location as indicated in Figure 5, combined with the lateral acceleration contours in Figure 15 and Figure 17 showing lower lateral accelerations for low spectral peak periods for OC3-Hywind.
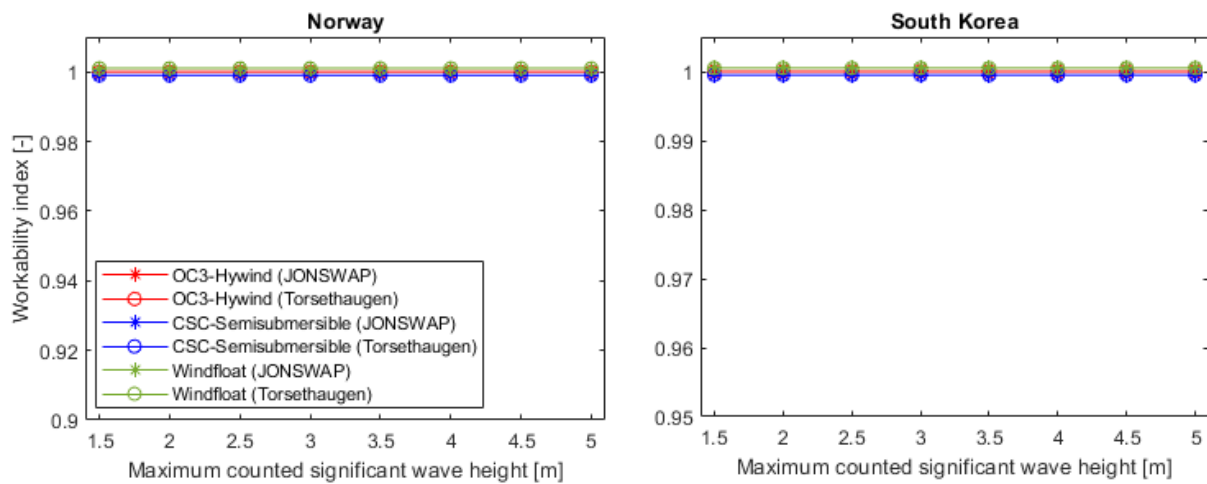

Figure 19. *Platform level* workability index for OC3-Hywind (red), CSC-Semisubmersible (blue), and WindFloat (green) using the JONSWAP (circle) and Torsethaugen (asterisk) wave spectra for a location in Norway (left) and South Korea (right).

Figure 20. *Nacelle level* workability index for OC3-Hywind (red), CSC-Semisubmersible (blue), and WindFloat (green) using the JONSWAP (circle) and Torsethaugen (asterisk) wave spectra for a location in Norway (left) and South Korea (right).
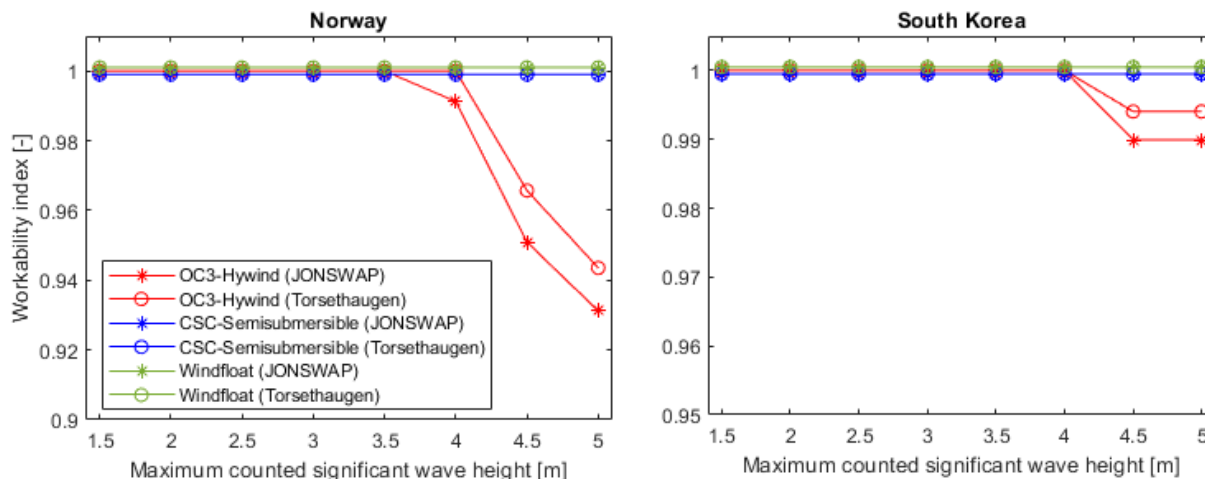
6. Conclusions

Three well-defined 5 MW floating wind concepts, i.e., OC3-Hywind (spar buoy), CSC Semisubmersible (semisubmersible) and WindFloat (semisubmersible), have been analysed with respect to human exposure to motion during maintenance operations. The relevant motion response criteria are based on root mean square values of lateral and vertical accelerations, and pitch motions.

The three floating wind concepts exhibit very different motion characteristics although their natural periods are not very different. Dynamic properties of the concepts such as the vertical position of the center of rotation, the phase angle between surge and pitch motion, and wavelengths corresponding to horizontal loading in phase or 180 degree out of phase on the different columns of the floaters for different wave directions can to a large extent describe the observed characteristics.

The effect of upscaling of the 5 MW semisubmersible concepts are investigated with respect to horizontal wave loads in phase on the different columns. When the scale is increased the wave periods leading to horizontal wave loads in phase on the columns will increase, and also more wave periods will enter the wave period range above 3 seconds. In total, this indicate that the impact of horizontal wave loads in phase on the columns of semi-submersible FOWTs will increase with scale.

Contour response plots of the relevant motion response criteria for work at the nacelle level and at the platform level are calculated for a generic load case matrix for a range of relevant spectral peak periods and significant wave heights using both the single peaked JONSWAP and the double peaked Torsethaugen wave spectra. The main findings from the response contour plots are:

- Only the lateral acceleration limit can potentially be exceeded for the three floating wind concepts considered.
- The lateral accelerations are generally reduced when using the double peaked Torsethaugen wave spectrum compared to using the single peaked JONSWAP spectrum.
- The lateral acceleration contour for OC3-Hywind has a quite flat curve as function of spectral peak period, while both semisubmersible concepts exhibits several peaks and troughs that typically corresponds with wavelengths with horizontal loading in or out of phase on the columns.
- The lateral accelerations of OC3-Hywind and CSC-Semisubmersible are significantly larger at the nacelle level than on the platform level, while it is the other way around with WindFloat, partly due to a high center of rotation above the nacelle level in an important frequency range. This implies that a person exposed to motion sickness onboard OC3-Hywind or CSC-Semisubmersible should seek towards the platform level to recover, while a person onboard WindFloat should seek towards the nacelle level.
- Overall, the CSC-semisubmersible has the lowest lateral acceleration level at the platform and nacelle levels, but the lateral accelerations at the nacelle level for WindFloat are smallest among the concepts for wave headings from 30 degrees (and 90, 150, 210, 270 degrees) due to wave loading out of phase on the columns for wavelengths corresponding to the horizontal distance between the columns.

The concept of a workability index is utilised to present the performance of the different floating wind concepts with respect to exposure of maintenance personnel to motion. The workability index for the three floating wind concepts are calculated for the nacelle and platform levels using both the JONSWAP and Torsethaugen wave spectra for two locations relevant for floating wind deployment. A reduced set of load cases (~500 cases) have been selected with a good representation of the distributions for significant wave height, spectral peak period, and wave heading for the coasts of Norway and South Korea. The main finding is that the workability index is equal to 1, for both the platform and nacelle level, regardless of concept, location, and wave spectrum used in the analyses, for significant wave heights up to 3.5 m which corresponds to the maximum significant wave height for crew transfers to FOWTs.

7. Acknowledgement

References

[1] W. Musial, "NREL," 2 April 2020. [Online]. Available: https://www.nrel.gov/news/program/2020/floating-offshore-wind-rises.html.

[2] A. Hopstad, K. Ronold and J. Slätte, "Design Standard for Floating Wind Turbine Structures," in *10th Deep Sea Offshore Wind R&D Conference*, Trondheim, 2013.

[3] B. Skaare, F. Nielsen, T. Hanson, R. Yttervik, O. Havmøller and A. Rekdal, "Analysis and measurements from the Hywind Demo floating wind turbine," *Wind Energy,* 2015.

[4] D. Roddier, C. Cermelli, A. Aubault and A. Peiffer, "Summary and Conclusions of the Full Life-Cycle of the WindFloat FOWT Prototype Project," in *International Conference on Offshore Mechanics and Arctic Engineering*, Trondheim, Norway., 2017.

[5] QFWE, "Global Floating Wind. Market and Forecast Report. 2021-2034," Quest Floating Wind Energy, 2021.

[6] B. Hu, P. Stumpf and W. van der Dejil, "Annual Offshore Wind Access Report," TNO, 2019.

[7] 4COffshore, "4coffshore," 4C Offshore, [Online]. Available: https://www.4coffshore.com/support/an-introduction-to-crew-transfer-vessels-aid2.html. [Accessed 2021].

[8] M. Scheu, D. Matha, M.-A. Schwarzkopf and A. Kolios, "Human exposure to motion during maintenance on floating offshore wind turbines," *Ocean Engineering,* no. 165, pp. 293-306, 2018.

[9] H. M. Gomes and D. Savionek, "Measurement and evaluation of human exposure to vibration transmitted to hand-arm system during leisure cyclist activity," *Brazilian Journal of Biomedical Engineering,* vol. 4, no. 30, pp. 291-300, 2014.

[10] N. J. Mansfield, Human response to vibration, New York: CRC Press , 2005.

[11] NORDFORSK, The Nordic Cooperative Project, Seakeeping Performance of Ships Assessment of a Ship's Performance in a Seaway, Trondheim: Marintek, 1987.

[12] K. Hasselmann, T. Barnett, E. Bouws, H. Carlson, D. Cartwright, K. Enke, J. Ewing, H. Gienapp, D. Hasselmann, P. Kruseman, A. Meerburg, P. Müller, D. Olbers, K. S. W. Richter and H. Walden, "Measurements of Wind-Wave Growth and Swell Decay during the Joint North Sea Wave Project (JONSWAP)," *Deutsche Hydrographische Zeitschrift,* no. 12, 1973.

[13] K. Torsethaugen and S. Haver, "Simplified double peak spectral model for ocean waves," in *ISOPE* , Touson, 2004.

[14] R. M. M. J. A. L. I. Guanche, "Walk-to-work accessibility assessment for floating offshore wind turbines," *Ocean Engineering,* pp. 216-225, 2016.

[15] DNV, "GeniEUser Manual. Vol. 1 - Concept design and analyses of offshore structures," 2016.

[16] DNV, "Wadam User Manual. Wave analysis by diffraction and Morison theory," 2014.

[17] DNV GL, "DNVGL-CG-0130," DNV GL, 2018.

[18] DNV GL, "DNV-RP-C205," Det Norske Veritas, 2010.

[19] DNV GL, "DNV-RP-H103," Det Norske Veritas, 2011.

[20] F. Çakıcı, B. Yıldız and A. D. Alkan, "Crew Comfort Investigation for Vertical and Lateral Responses of a Container Ship," in *12th International Conference on the Stability of Ships and Ocean Vehicles*, Glasgow, 2015.

[21] I. S. Dolinskaya, M. Kotinis, M. G. Parsons and R. L. Smith, "Optimal Short-Range Routing of Vessels in a Seaway," *Journal of Ship Research,* vol. 53, no. 3, pp. 121-129, 2009.

[22] P. R. Payne, "On quantizing ride comfort and allowable accelerations," in *AIAA/SNAME Advanced Marine Vehicles Conference*, 1976.

[23] International Organization for Standardization, "ISO 2631/3," ISO, Geneva, 1985.

[24] J. Jonkman, S. Butterfield, W. Musial and G. Scott, "Definition of a 5-MW Reference Wind Turbine for Offshore System Development," National Renewable Energy Laboratory, 2009.

[25] J. Jonkman, "Definition of the Floating System for Phase IV of OC3," National Renewable Energy Laboratory, 2010.

[26] C. Luan, Z. Gao and T. Moan, "Design and analysis of a braceless steel 5-mw semi-submersible wind turbine," in *35th International Conference on Ocean, Offshore and Arctic Engineering*, Busan, 2016.

[27] D. Roddier, A. Peiffer, A. Aubault and J. Weinstein, "A generic 5 MW WindFloat for numerical tool validation & comparison against a generic spar," in *Proceedings of the ASME 2011 30th International Conference on Ocean, Offshore and Arctic Engineering*, Rotterdam, 2011.

[28] C. Luan, V. Chabaud, E. E. Bachynski, Z. Gao and T. Moan, "Experimental validation of a time-domain approach for determining sectional loads in a floating wind turbine hull subjected to moderate waves," in *14th Deep Sea Offshore Wind R&D Conference, EERA DeepWind'2017*, Trondheim, 2017.

[29] B. Skaare, Hanson, T.D., F. Nielsen, R. Yttervik, A. Hansen, K. Thomsen and T. Larsen, "Integrated dynamic analysis of floating offshore wind turbines," in *EWEC 2007 - European Wind Energy Conference & Exhibition*, Milano, 2007.

[30] O. M. Faltinsen, Sea Loads on Ships and Ocean Structures, Cambridge: Cambridge University Press, 1990.

Chapter 4

4. Additional Investigations and Results

In this chapter investigations and results which were not included in **Paper I: Analysis of spar and semi-submersible floating wind concepts with respect to human exposure to motion during maintenance operation** is presented. The chapter starts with the validation of the potential theory by checking the dimensionless numbers of the flow around the submerged bodies. Later, an investigation on the difference between the motions of the floaters in the dominant wave direction and the motions on the defined degree of freedoms is presented. Lastly, the chapter is finished with the expected extreme instantaneous motions on the floaters based on the duration of the work.

4.1. Validation of linear potential theory for the chosen floaters

Flows around the cylinders of all floaters are theoretically investigated by checking dimensionless parameters such as Keulegan-Carpenter Number (KE) and Reynold Number (RE) as given in Equation **(4.1)** and **(4.2)**. To determine if flow separation and turbulence occur around the cylinders, KC and RE numbers are calculated along with the depth of all designs for defined periodic sea states as shown in **Figure 4.1**. The periodic sea states are taken from The Douglas Scale which is a method to describe the sea condition from 0 (calm) to 8 (extreme) according to its wave height and wave period [32]. The defined sea states in The Douglas Scale are listed in **Table 3**.

Table 3: Periodic sea states of The Douglas Scale.

Sea States	1	2	3	4	5	6	7	8
H [m]	0.09	0.67	1.40	2.44	3.66	5.49	9.14	15.24
T [s]	2.0	4.8	6.5	8.1	9.7	11.3	13.6	17.0

$$KC = \frac{VT}{D} \tag{4.1}$$

$$RE = \frac{VD}{\nu} \qquad \text{(4.2)}$$

Flow separation occurs when KC is greater than 2 and flow around the cylinder becomes viscous dominated, therefore potential theory cannot be applied in such region. Flow separation around the OC3-Hywind only occurs at the upper parts of the floater at the extreme sea states, while flow separation takes place all along CSC-Semisubmersible's and WF's vertical columns at the sea states 7 and 8. Considering, wind farm operators usually conduct crew transfer operations on the weather windows where the highest significant wave height (H_s) is below 3.5 m [5], potential flow theory is valid for this study since floaters do not experience flow separation when only excited by the waves with H_s below 3.5 m.

The flow is considered turbulent and the viscous-drag term becomes non-negligible in the conditions where $RE > 10^5$. Flow around both OC3-Hywind, CSC-Semisubmersible and WindFloat have larger $RE > 10^5$ in many sea states. Therefore, to apply linear potential theory, defined additional linear damping matrices are implemented to hydrodynamic models to compensate the viscous-drag term from Morison's equation, as recommended in the definition reports of the floaters [5], [22], [23].
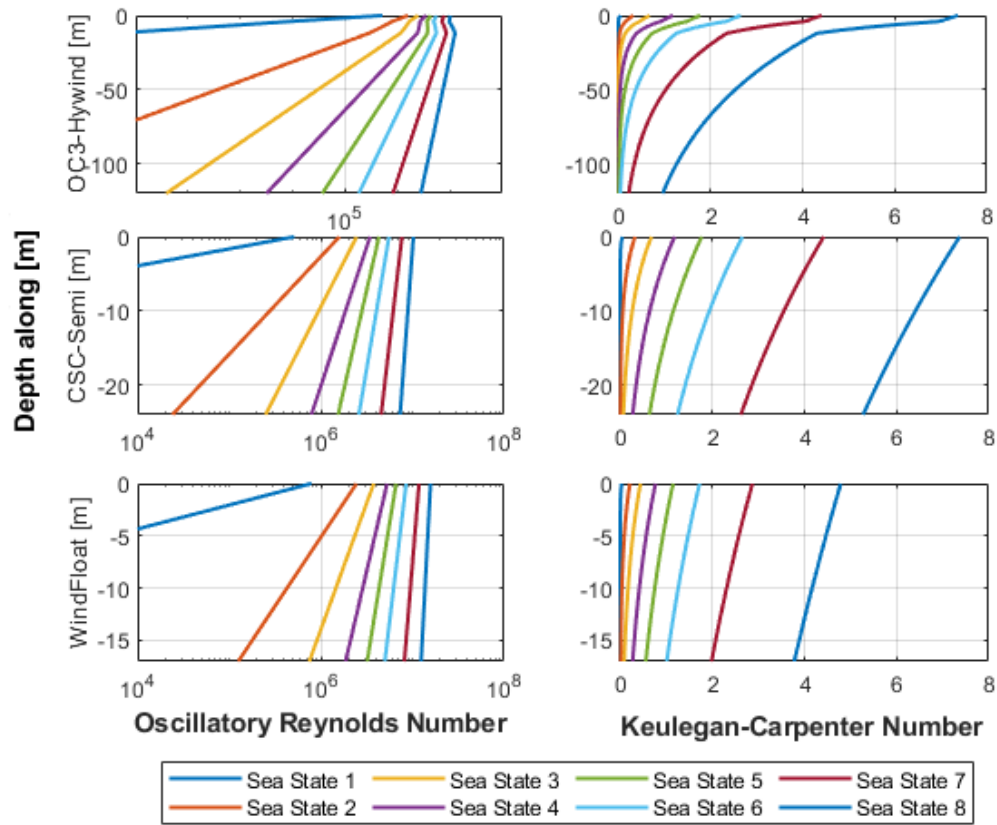
Figure 4.1: Dimensionless parameters Re number (left), KC number (right) of OC3-Hywind (top), CSC-Semisubmersible (middle) and WindFloat (bottom) in the sea states defined by The Douglas Scale.

4.2. Investigation of the motions on the dominant wave direction

Maximum motions are expected to occur on the floater in line with the wave direction and used software gives only the motions on the body in line with the axes of the defined coordination system. Hence, for wave headings β different than defined horiztontal axes of the coordination system ($\beta \neq 0, 90, 180, 270, 360$), results do not present the maximum motions experienced on the bodies. Therefore, bodies must be rotated around the z-axis to calculate the maximum motions on the body in the corresponding wave directions. The precision of the calculated response amplitude operators (RAOs) is investigated for the load cases with wave headings that are in between the directions of global DOFs of the floating bodies. One of the study cases, CSC-Semisubmersible, whose geometry and configuration explained earlier, is chosen for the investigation. Surge/Sway and Pitch/Roll RAOs of the model on its original arrangement that is excited by the regular waves with 50 degrees of heading is compared with the Surge and Pitch RAOs of the 50 degrees rotated body that is excited by waves propagating along the x-axis, see **Figure 4.2**. Differences are found significant. Therefore, several FEM models are created for each floater by rotating floaters around its vertical centerline (CL) to calculate the RAOs of the dominant motion for different wave headings. Bodies are rotated with the steps of 10 degrees until the symmetry of the floater is accomplished, in terms of its geometry and mooring configurations. Since global coordination system *(x)* is kept unchanged, mass and mooring stiffness matrices of each rotated floater are transformed into its new coordination system *(x')* by using the transformation matrix *(R)* for each rotation (ψ) around its z axis **(4.3)** [33].

$$x' = Rx \qquad R = \begin{bmatrix} R_{z,\psi} & 0^{3x3} \\ 0^{3x3} & R_{z,\psi} \end{bmatrix} \qquad R_{z,\psi} = \begin{bmatrix} cos\psi & -sin\psi & 0 \\ sin\psi & cos\psi & 0 \\ 0 & 0 & 1 \end{bmatrix}$$

$$\left(M_{ij} + A_{ij}\right)R^T R\ddot{x}_{ij} + B_{ij}R^T R\dot{x}_{ij} + C_{ij}R^T Rx_{ij} = F_{ij}$$

$$\left(M_{ij} + A_{ij}\right)R^T \ddot{x}'_{ij} + B_{ij}R^T \dot{x}'_{ij} + C_{ij}R^T x'_{ij} = F_{ij}$$
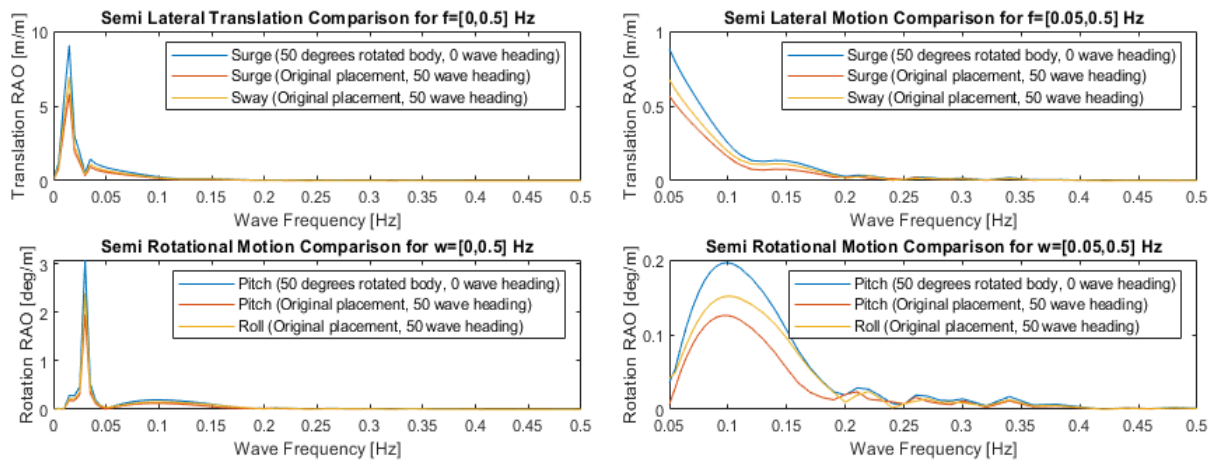
(4.3)

Figure 4.2: Comparison of the lateral and rotational motions experienced on the CSC-Semisubmersible along the dominant wave direction and the defined degree of freedoms.

4.3. Expected extreme accelerations on the floaters

In this section, the expected extreme accelerations on the chosen reference models are demonstrated in contour plots for different reference periods and locations on the platform. 3 hours reference time is recommended by DNV for the calculation of short-term statistical motions of floating vessels in the irregular sea states [16], [34]. Also, it is stated by Scheu et. al. that typical maintenance activity on the floaters takes approximately 10 hours [5]. Additionally, the nacelle and the platform are the two locations maintenance personnel spend their time the most onboard. Therefore estimated expected lateral and vertical accelerations at the nacelle and the platform level of the floaters are calculated for 3 hours and 10 hours reference time in the generated load cases. The range of the generated load cases is chosen as follows:

$$0.5 < H_s < 5 \, m$$

$$3 < T_p < 10 \, m$$

$$(4.4)$$

The range shown in Equation **(4.4)** represents the 90% confidence interval of H_s, T_p values from the hindcast data of both study sites. Later, estimated extreme motions are assessed against the ISO2631/1 which is a comfort grading standard for instantaneous accelerations experienced by humans [31].

4.3.1. 3 hours reference period

Irregular sea states remain stationary over time intervals of 2 to 3 hours [15]. Therefore extreme accelerations expected on the nacelle and the platform level of the floaters is calculated for 3 hour reference period. Load cases are defined with 0 degree wave heading and modelled with JONSWAP spectrum. Expected exterme accelerations at the nacelle and platform level of the chosen desings are demonstrated in **Figure 4.3** and **Figure 4.4**, respectively. Results reveal that expected extreme vertical accelerations at the nacelle and platform level remain in the comfortable zone according to ISO2631/1 for all chosen floaters. However, lateral accelerations at the nacelle level may reach an extremely uncomfortable level ($a < 2 \, m/s^2$) [31] for all floaters while it may also reach a very uncomfortable level ($a < 1.25 \, m/s^2$) [31] at the platform level of OC3-Hywind and WindFloat. Besides, results also show that expected extreme lateral accelerations, even if they are instantaneous, they are expected to be fairly

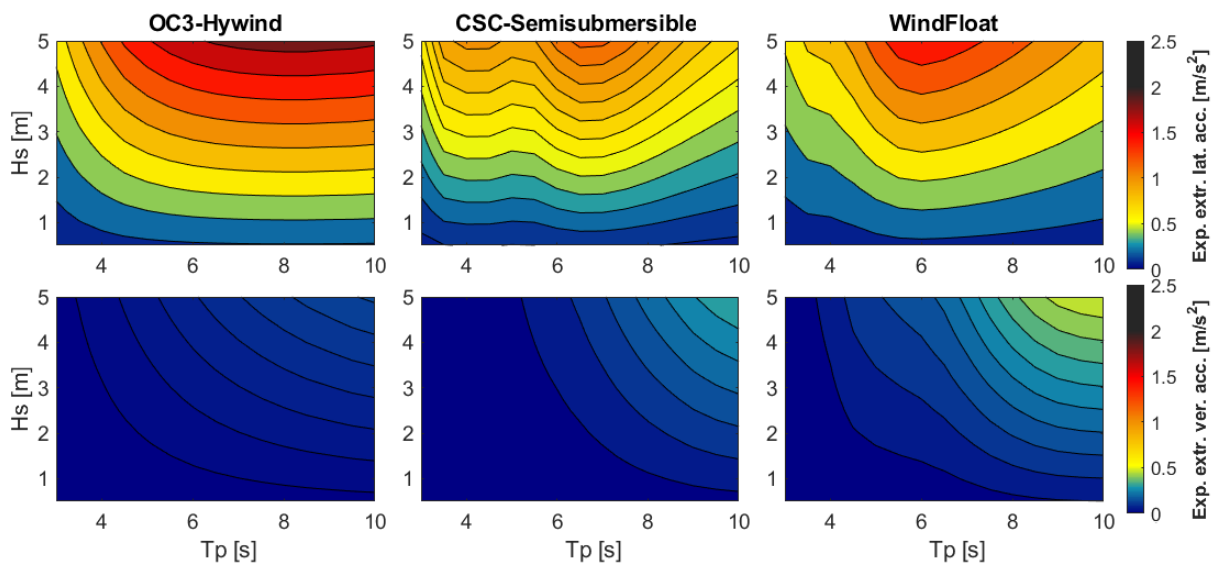uncomfortable for 3 hours reference period both the platform and the nacelle level of all chosen floaters.

Figure 4.3: Extreme expected lateral (top) and vertical (bottom) accelerations at the nacelle level of OC-Hywind (left), CSC-Semisubmersible (middle), WindFloat (right) in 3 hours reference time.
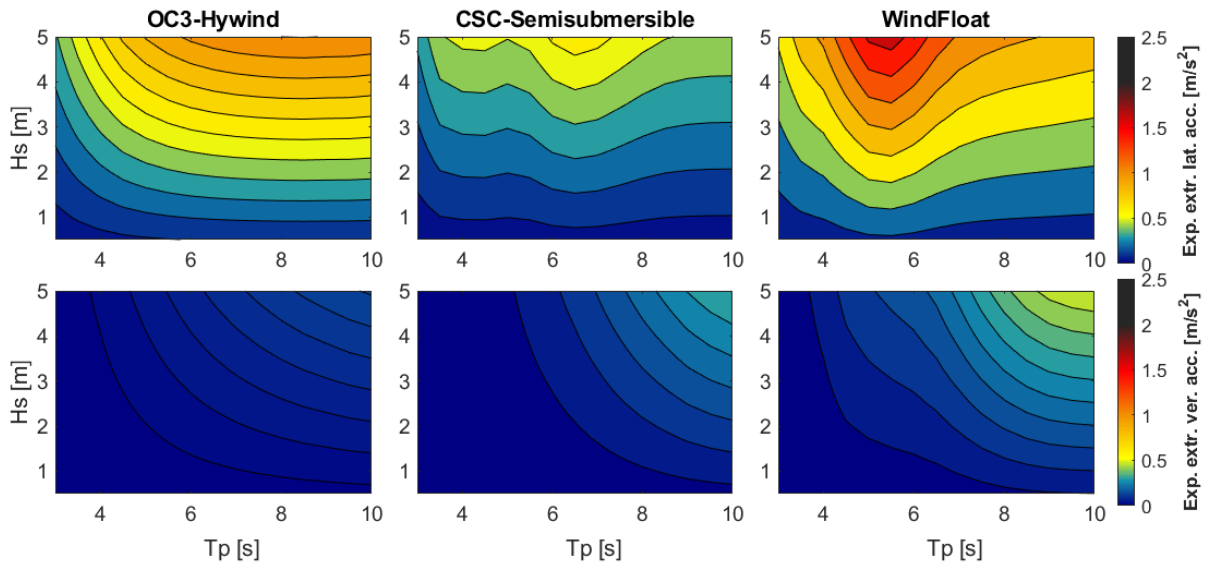

Figure 4.4: Extreme expected lateral (top) and vertical (bottom) accelerations at the platform level of OC-Hywind (left), CSC-Semisubmersible (middle), WindFloat (right) in 3 hours reference time.

4.3.2. 10 hours reference period

Maintenance activity on FOWTs approximately takes 12 hours as a combination of 2 hours on the transfer vessel and 10 hours on the floater (inspection, fault-finding, component changing, etc.) [5]. Accordingly, the extreme expected accelerations at the nacelle and platform level of

the chosen floaters are calculated for 10 hours reference time under the head waves that are modelled with JONSWAP spectrum and shown in **Figure 4.5** and **Figure 4.6** respectively. As in the 3 hours reference period, the vertical accelerations at any location of all floaters remain comfortable for the humans located on the structure according to ISO-2631/1. Naturally, the expected lateral accelerations in 10 hours reference time reach higher levels than the lateral accelerations in 3 hours. Results also reveal that instantaneous accelerations at the nacelle and the platform level of all floaters may reach extremely uncomfortable level $(a < 2\ m/s^2)$ according to ISO-2631/1 [31].
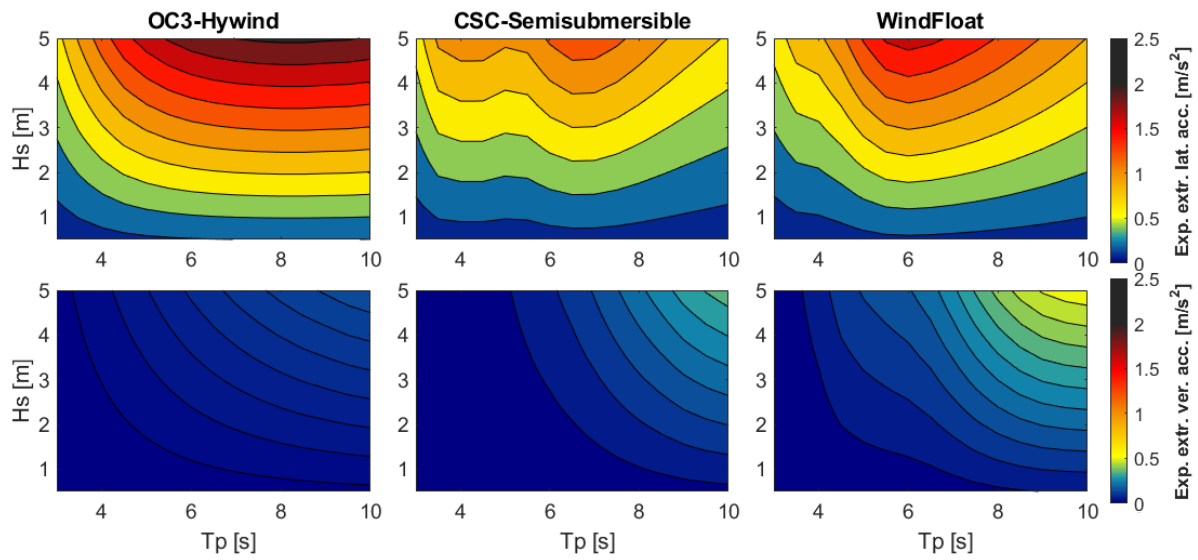
Figure 4.5: Extreme expected lateral (top) and vertical (bottom) accelerations at the nacelle level of OC-Hywind (left), CSC-Semisubmersible (middle), WindFloat (right) in 10 hours reference time.
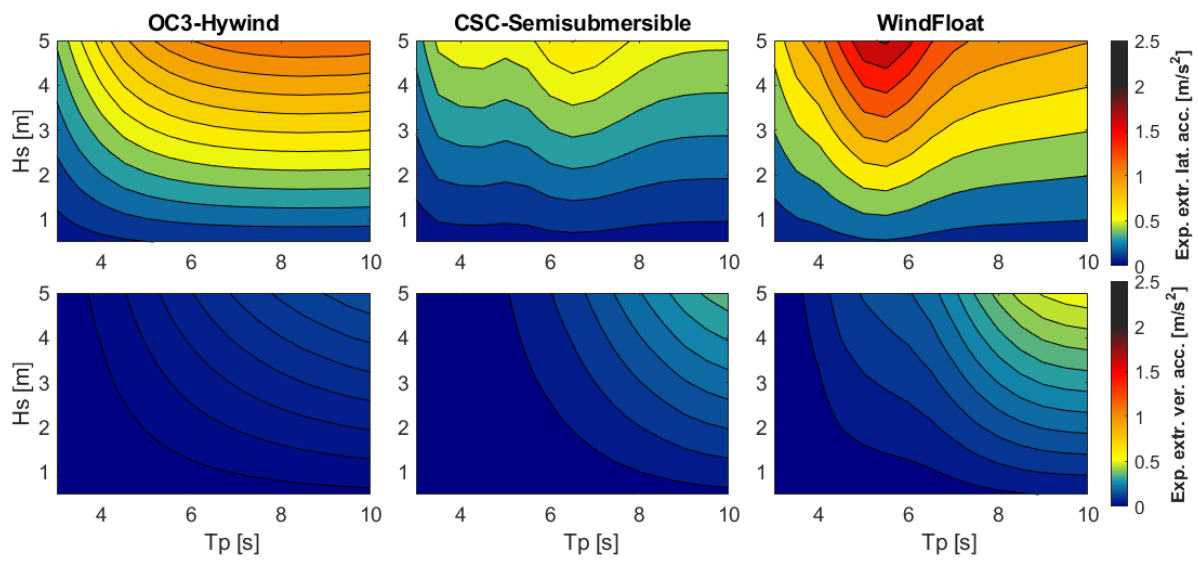

Figure 4.6: Extreme expected lateral (top) and vertical (bottom) accelerations at the platform level of OC-Hywind (left), CSC-Semisubmersible (middle), WindFloat (right) in 10 hours reference time.

References

[5] M. Scheu, D. Matha, M.-A. Schwarzkopf, and A. Kolios, 'Human exposure to motion during maintenance on floating offshore wind turbines', *Ocean Engineering*, vol. 165, pp. 293–306, Oct. 2018, doi: 10.1016/j.oceaneng.2018.07.016.

[15] DNV GL, 'DNV-RP-C205: Environmental Conditions and Environmental Loads', *DNV-RP-C205: Environmental Conditions and Environmental Loads*, p. 124, 2010.

[16] DNV GL, 'DNVGL-CG-0130 Wave loads', *DNVGL-CG-0130 Wave loads*, p. 84, 2018.

[22] J. Jonkman, 'Definition of the Floating System for Phase IV of OC3', NREL/TP-500-47535, 979456, May 2010. doi: 10.2172/979456.

[23] C. Luan, Z. Gao, and T. Moan, 'Design and analysis for a steel braceless semi-submersible hull for supporting a 5-MW horizontal axis wind turbine', p. 296, 2016.

[31] ISO, 'ISO 2631-1: Mechanical vibration and shock'. 1997.

[32] T. Fossen, *Handbook of Marine Craft Hydrodynamics and Motion Control*. 2011. doi: 10.1002/9781119994138.

[33] DNV GL, 'DNV-RP-H103: Modelling and Analysis of Marine Operations', *DNV-RP-H103: Modelling and Analysis of Marine Operations*, p. 150, 2011.

5. Conclusions and Recommendations

5.1. Conclusions

The conclusions based on the findings presented in Chapter 3 and Chapter 4 can be formulated as follows:

1. **Dynamic properties of the chosen floaters:**

    Motions that occur on the three chosen floating concepts show significant variation in terms of their characteristics even though their natural periods are not too different. Based on the RAOs derived from the motion response analysis in the frequency domain with a potential theory code, horizontal loadings on the platforms are found positively correlated with the wave periods which is in phase on the different columns, especially for semisubmersible concepts. Besides, the effect of mooring lines on the floater motions relevant to the comfort of personnel on the structure are seemed not significant, since acceleration responses on the floaters are quite symmetrical for the wave headings in phase with geometrical symmetry. Lastly, all floaters have higher peaks of horizontal accelerations on their nacelle compared to the platform level except WindFloat. This can be explained by the vertical position of its centre of rotation which is found related to the phase difference between its surge and pitch motions at the platform level.

2. **Estimated short-term statistical motions of the floaters:**

    Based on the contour plots of r.m.s. responses of each concept loaded with generic load cases, the lateral acceleration is found as the only parameter exceeding the chosen limiting criteria for human exposure to motions. Further, the motion responses are found sensitive for the chosen spectral model for the lower wave periods due to the second peak of the Torsethaugen spectrum. Additionally, larger responses are expected to occur on OC3-Hywind at the coast of Norway compared to South Korea, since Norway's hindcast data contains a higher rate of waves with a longer wave period. Consequently, OC3-Hywind have approximately 99% workability for the site in South Korea and drops to

approximately 93% for the site in Norway. The main finding is that the workability index is equal to 1, for both the platform and nacelle level, regardless of concept, location, and wave spectrum used in the analyses, for significant wave heights up to 3.5 meters - corresponding to the maximum significant wave height for crew transfers to FOWTs.

5.2. Recommendations

Further work within this field could include:
- Considering other concepts than spars and semisubmersible floating wind concepts. The impact of horizontal wave loading in phase on structures with distributed geometry in the wave zone could be of particular interest based on the findings in the present study.
- Time-domain simulations where directional effects from wind and swell sea can be taken into account.
- Research on relevant motion response criteria adapted to the nature of the maintenance work onboard a floating wind turbine, such as a ~10 hours work period with a combination of physical and intellectual work.
- Analyses of FOWTs of a larger scale than in the present study.